5 Results and Discussion

5.1 Catalyst Preparation

5.1.1 Synthesis of undiluted MoVTeNb precursor

In the preparation of catalyst, the selections of right precursors are important and should be done carefully, because the formation of slurry affects the catalyst structure and catalytic performance. The preparation of MoVTeNb oxide follow three well established common steps for metal oxide synthesis: (a) admixing of starting materials to form a slurry mixture; (b) removal of water to obtain a dry catalyst precursor (solidification); (c) heat treatment (calcination) of catalyst precursor to form oxide catalysts. This chapter will focus on the synthesis procedure and the characterization techniques of the precursor and oxide catalyst. The main steps involve in the preparation of catalysts is first to deposit the active component precursor as a divided form on the support. Then, the precursor will transform into the required active component. In the case of supported catalysts, the silica does not play a major role of an active support but rather that of a diluent or spacer because of the 50: 50 wt% loading between the active component and the support. The synthesis procedures are discussed in details in Section 3.2.3 and 3.2.4 and was done using LabMax reactor. During the preparation of catalyst, temperature, pH, turbidity and other parameters are determined based on starting material added. However, this study of parameters variety does not come into play as it is limited by the COMBICAT department in terms of developing and optimizing the preparation of MoVTeNb oxides catalyst (Abdullah 2004; Cut Aja 2004; Idris 2004)

$Mo_1V_{0.3}Te_{0.23}Nb_{0.12}Ox$ catalysts were synthesized from aqueous slurry according to the patented procedure (Ushikubo, Nakamura et al. 1995). The procedure is illustrated in Section 3.3 (Scheme 3.2). Figure 5.1 and 5.2 clearly show the color changes in MoVTeNb slurry synthesis and was done *in-situ by using* LabMax reactor which is monitored by a computer. The details of the *in-situ* graph are summarized in Table 5.1. During the preparation of catalyst, all the parameters such as temperature, pH, turbidity and conductivity were monitored. Starting from the addition of ammonium heptamolybdate into bi-distilled water and heated up from 303 to 353 K, the pH decreases from 6.17 to 5.43. The decrease in pH is accompanied by a partial transformation of ammonium heptamolybdate to ammonium octamolybdate. When a dissolved ammonium metavanadate (AMV) is added to the solution of AHM at 353 K (pH 5.43) the pH increases to 5.79 and significant changes in the Raman spectrum are observed [Beato et al, 2006]. The turbidity of the solution increased from 10.82% up to 66.52% which turns the color of solution from cloudy yellow to clear yellow. Tyndall effect was observed in this solution whereas the precipitation occurs during AMV addition. This observation strongly indicates chemical interaction between AHM and AMV in the mixed solution. Based on the knowledge generated using molybdenum model systems to the complex system, the role of vanadium is identified as the linking element between isomerising octamolybdate species.

The subsequent addition of hexaoxotelluric acid at 353 K is accompanied by a pH drop from 5.79 to 5.68 and a color change from clear yellow to dark red. This could be assigned to terminal V=O bonds of protonated decavanadate species $[H_xV_{10}O_{28}]^{(6-x)-}$ from the Raman spectrum. This is the reason why the normalized pH traces are different, especially when cations are changed. Then, finally the strongly acidic (pH niobium solution = 0.8, T= 296 K) niobium oxalate solution is added to the ternary mixture of Mo, V and Te at 313 K, the

pH drops to 3.62 and a precipitate was formed after an induction period of several seconds. As the slurry formation is delayed by about one minute, an effect primarily due to the pH shift is unlikely; it is rather believed that Nb acts as a precipitating agent, after the Nb complex is destroyed in a kinetically controlled step. The turbidity of the solution was increased to 99 % when agglomeration started and become slurry. At this stage, Tyndall effect was observed where the formation of small particles in the solution. The slurry was aged for 1 hour at 313 K and cooled it down at 303 K before proceed to the next step. The slurry was then immediately introduced to the spray dryer to be solidified into powder. The key step identified in the model system, namely the isomerisation reaction between α and ß octamolybdate is essential in MoVTeNbOx preparation procedure or any other complex catalytic system containing molybdenum. Therefore, the structure formation depends strongly on the treatment parameters during isomerisation stage i.e., the temperature or on the metal salt solution added during isomerisation. The understanding towards the preparation of catalyst is growing with every treatment parameter studied.

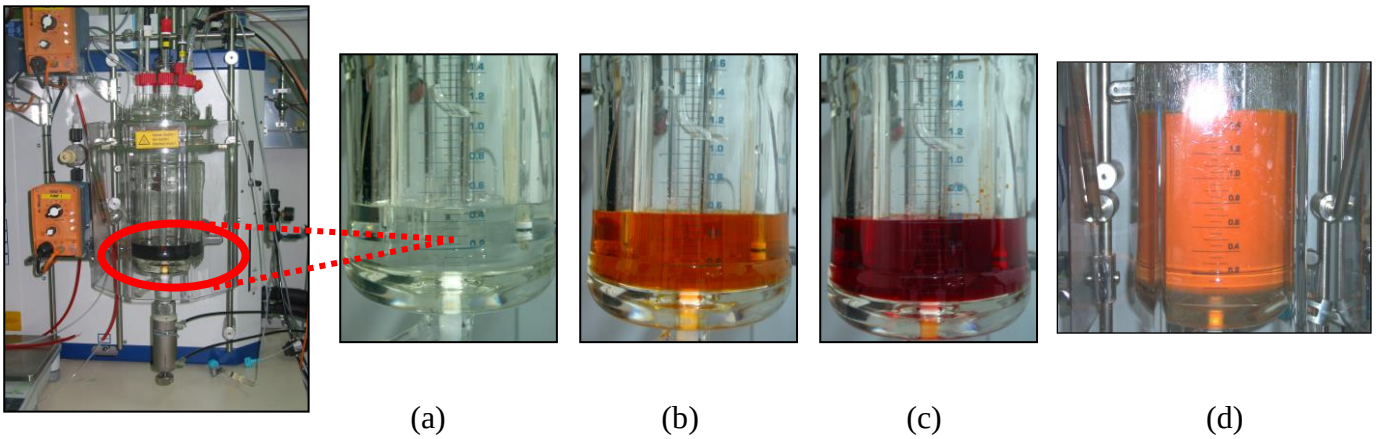

(a) (b) (c) (d)

Figure 5.1: In-situ LabMax dried precursor. (a) Ammonium heptamolybdate heat up to 353 K, (b) Addition of Ammonium metavanadate at same temperature, (c) Addition of Telluric acid at 353 K and (d) Formation of slurry after adding Niobium oxalate solution at 313 K.

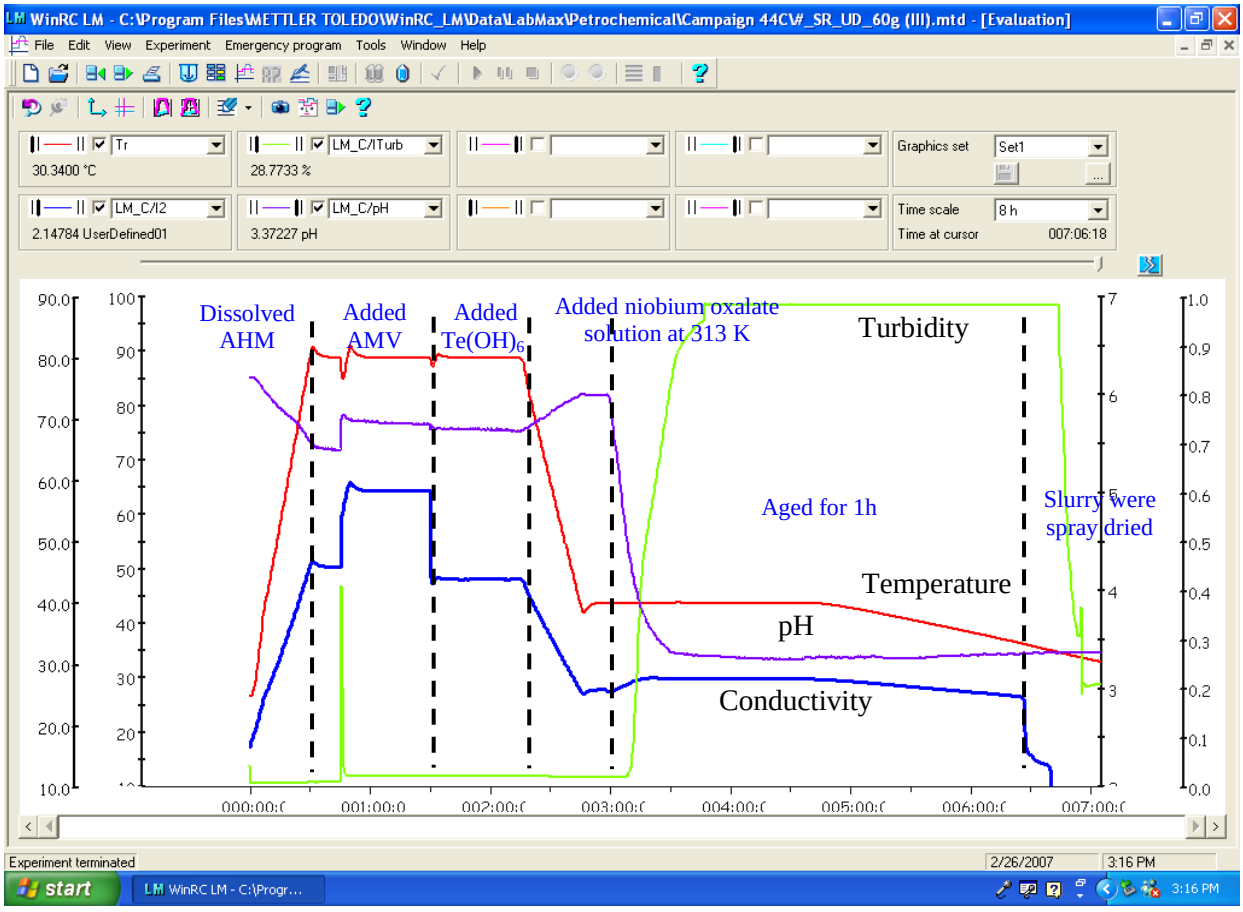

Figure 5.2: Plot of different measurements recorded during the preparation of catalyst using Labmax**.**

Table 5.1 Readings of different measurements recorded for $Mo_1V_{0.30}Te_{0.23}Nb_{0.125}$ synthesis with in-situ LabMax

Process	Salt Precursor	Temperature (K)	pH (adding salt)	Turbidity (%)	Conductivity (%)	Observations
Solution 1	AHM	353	5.43	10.79	50.62	**Colorless**
	AMV	353	5.42	10.82	50.35	**Yellow cloudy to clear yellow**
	AMV	351	5.71	66.52	59.39	
	AMV	349	5.79	25.83	60.04	
	AMV	353	5.73	12.00	64.35	
	Te Acid	352	5.67	11.92	47.75	**Dark red clear**
	Te Acid	353	5.64	11.87	48.08	
Decrease to 313		348	5.67	11.88	45.47	**Remain as clear dark red solution**
		312	5.99	11.71	27.21	
		313	5.91	11.71	27.39	
		313	3.33	98.60	29.83	
Adding solution 2	Nb oxalate solution	313	3.35	99.01		**Orange slurry**
Ageing 1 hour		**313**	**3.31**	**98.58**	**29.81**	**Thick Orange slurry**

5.1.2 In-situ Raman spectroscopy on solutions

In order to elucidate chemical processes during the synthesis of the precursor, the reaction involved in the early preparation was monitored by in-situ Raman spectroscopy. The Raman spectra of reference solutions are represented in Figure 5.3. As mentioned above, the pH decreases when the starting material is dissolved in bi-distilled water. This is due to the partial transformation of ammonium heptamolybdate to ammonium octamolybdate. The dependency between pH and temperature is well known for the given concentration (Pope 1983) and can be detected in the Raman spectrum with the appearance of a shoulder peak at 955 cm^{-1} [Figure 5.2] (Aveston, E.W.Anacker et al. 1964; Mestl and Srinivasan 1998). However, heptamolybdate still remains in the main species at 353 K with its characteristic Mo=O stretching bands at 937 and 893 cm^{-1} (Figure 5.2 (a) and (b) (Tytko and Schonfeld 1975)).

Figure 5.3 (c) shows the spectrum of the light yellow ammonium metavanadate solution at 353 K (pH 5.7) which exhibits an intense peak at 944 cm^{-1} and a weak shoulder peak near 900 cm^{-1}. The two peaks are assigned to ν_{Vo2} (sym) and ν_{Vo2} (asym.) modes, respectively, of cyclic $(VO_3)_n^{n-}$ species which VO_2 units are linked by single oxygen bridges (Griffith and T.D.Wickins 1966).Such bands are observed even at pH range from 9.6 to 8 (Griffith and T.D.Wickins 1966). The single peak at 644 cm^{-1} in the spectrum of the colorless solution of hexaoxotelluric acid at 296 K (pH 3.7) is corresponding to the ν (TeO) vibrations (Gupta 1937).

Bands at 942, 919 and 570 cm^{-1} are assigned to Nb=O and Nb-O stretching vibrations, respectively, were observed with the ammonium niobium oxalate solution at 296 K and pH around 0.8 [Figure 5.3 (e), (Jehng and I.E.Wachs 1991)].

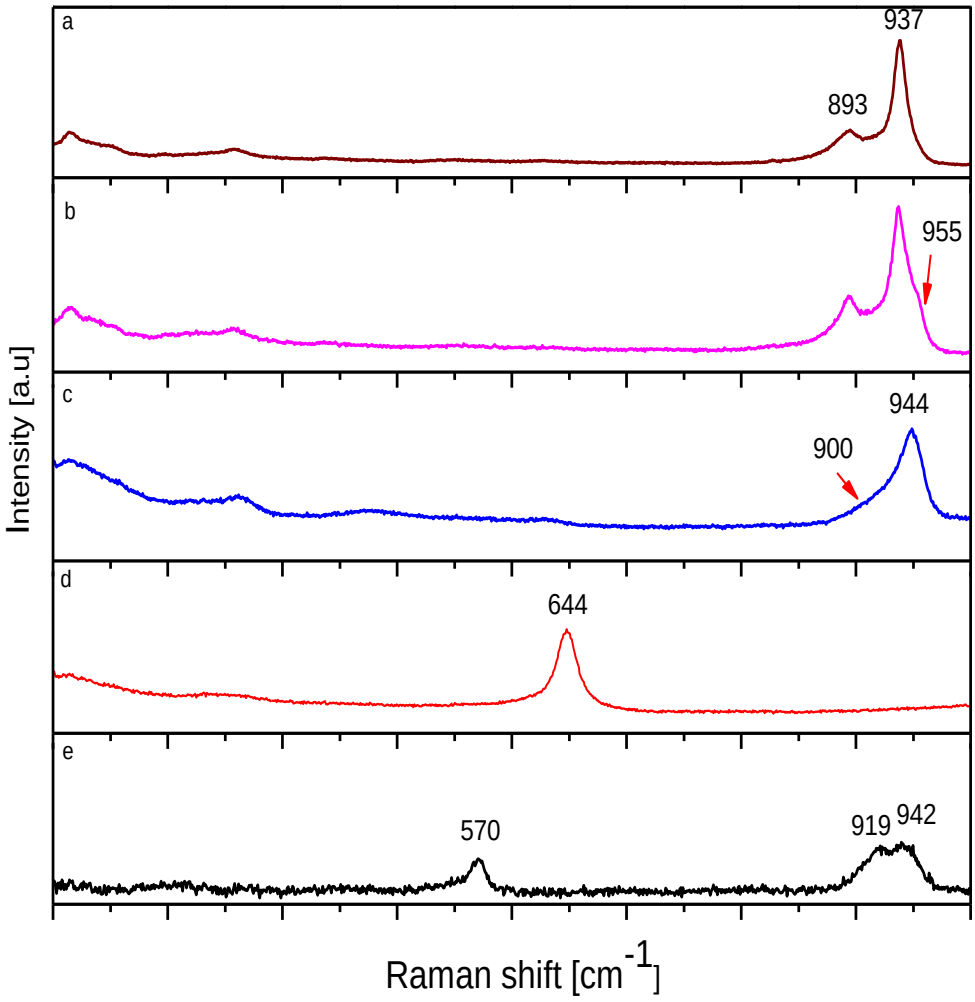

Figure 5.3: In-situ Raman spectra for aqueous solution of (a) AHM (pH 5.2, T=333K), (b) AHM (pH 5.0, T= 353 K), (c) AMV (pH 5.7, T=333 K), (d) $Te(OH)_6$ (pH=3.7, T=296 K) and (e) $(NH_4)_2Nb_2(C_2O_4)_5$ (pH=0.8, T=296 K)

Table 5.2: Summary of Raman band positions in aqueous solutions (Beato, A. Blume *et al*. 2006).

Solution	T (K)	pH	ν (cm^{-1})[a]	Assignment	Reference
AHM	333	5.2	937 (s) 893 (m)	ν (Mo=O)$Mo_7O_{24}^{6-}$	**Griffith et.al**
AHM	353	5.0	955 (sh)	ν (Mo=O)$Mo_8O_{26}^{4-}$	**Mestl g. et.al, Tytko K.H. et.al Griffith et.al**
			944 (s) 900 (sh)	ν (V=O) $[VO_3]_n^{n-}$	**Gupta J.**
$Te(OH)_6$	296	3.7	644 (s)	ν (Te-O)	**Jehng J.M. et.al**
$(NH_4)_2Nb_2(C_2O_4)_5$ (ANO)	296	0.8	570 (m)	ν (Nb-O)	**Griffith et.al**
			942 (s) 919 (s)	ν (Nb=O)	
AHM + AMV	353	5.5	980 (s)	ν (V=O) $[V_{10}O_{28}]^{6-}$	**Botto I.L. et.al**
			956 (m)		
			848 (m)	ν (V-O-O) or ν (Mo-O-V)	
AHM + AMV+ $Te(OH)_6$	353	5.0	1000 (m)	ν (V=O) $[H_xV_{10}O_{28}]^{(6-x)-}$	**Botto I.L. et.al**
			975 (vw)	Or ν (Mo=O) $[TeMo_5VO_{24}]^{7-}$	**Yuhao S. et.al**
			937 (s)	ν (Mo=O) $[TeMo_6VO_{24}]^{6-}$	**Anderson J.S. et.al**
			899 (m)		

Solution	T (K)	pH	ν (cm^{-1})[a]	Assignment	Reference
AHM	333	5.2	937 (s)	ν (Mo=O)$Mo_7O_{24}^{6-}$	**Griffith et.al**
			893 (m)		
AHM	353	5.0	955 (sh)	ν (Mo=O)$Mo_8O_{26}^{4-}$	**Mestl g. et.al, Tytko K.H. et.al Griffith et.al**
			944 (s)	ν (V=O) $[VO_3]_n^{n-}$	**Gupta J.**
			900 (sh)		
$Te(OH)_6$	296	3.7	644 (s)	ν (Te-O)	**Jehng J.M. et.al**
$(NH_4)_2Nb_2(C_2O_4)_5$ (ANO)	296	0.8	570 (m)	ν (Nb-O)	**Griffith et.al**
			942 (s)	ν (Nb=O)	
			919 (s)		
AHM + AMV	353	5.5	980 (s)	ν (V=O) $[V_{10}O_{28}]^{6-}$	**Botto I.L. et.al**
			956 (m)		
			848 (m)	ν (V-O-O) or ν (Mo-O-V)	
AHM + AMV+ $Te(OH)_6$	353	5.0	1000 (m)	ν (V=O) $[H_xV_{10}O_{28}]^{(6-x)-}$	**Botto I.L. et.al**
			975 (vw)	Or ν (Mo=O) $[TeMo_5VO_{24}]^{7-}$	**Yuhao S. et.al**
			937 (s)	ν (Mo=O) $[TeMo_6VO_{24}]^{6-}$	**Anderson J.S. et.al**
			899 (m)		

Figure 5.4 shows the Raman spectra of the mixed solutions. When solid AMV is added into the solution of AHM at 353 K the pH increases from 5.0 to 5.5. This significant change is observed in Raman spectrum which indicates a chemical interaction between AHM and AMV in the solution (Figure 5.4 (a)). It is worth mentioning that precipitation will occur if one decreases the pH of a pure AMV solution at 353 K with the same concentration as for the binary system from originally 5.7 to 5.5, precipitate will occur. However, the presence of the bands at 937 and 893 cm^{-1} corresponding to heptamolybdate ions and (VO_3) species, respectively, reveals that the unreacted single Mo and V components still dominate the system. The new bands appear at 980, 956 and 848 cm^{-1} can be assigned to a decavanadate ion $(V_{10}O_{28})^{6-}$, which is the main species in aqueous AMV solution at pH around 5.5 (Griffith and Lesniak 1966).

According to Beato and co-workers, the weak band at 848 cm^{-1} which is assigned for the decavanadate ion, may be assigned to asymmetric stretching vibrations of bridging Mo-O-V bonds of a mixed MoV compound (Beato, A. Blume et al. 2006). A summary of Raman bands assignation is tabulated in Table 5.2.

The Raman spectrum of the ternary MoVTe solution is shown in Figure 5.4 (b). The subsequent addition of hexaoxotelluric acid at 353 K is followed by a pH drop from 5.5 to 5.0 and color change from light orange to deep red. Bands in the high frequency range are observed at 1000, 937 and 899 cm^{-1}. The band at 1000 cm^{-1} could arise from terminal V=O bonds of protonated decavanate species $[H_xV_{10}O_{28}]^{(6-x)-}$ (Griffith and Lesniak 1966). The bands at 937 and 899 cm^{-1} fit very well to the powder Raman spectrum of the Anderson-type heteropolyanion $[TeMo_6O_{24}]^{6-}$ in the form of its ammonium salt (Botto, C.I. Cabello

et al. 1997). A schematic representation of Anderson-type species is given in Figure 5.5 (Anderson 1937).

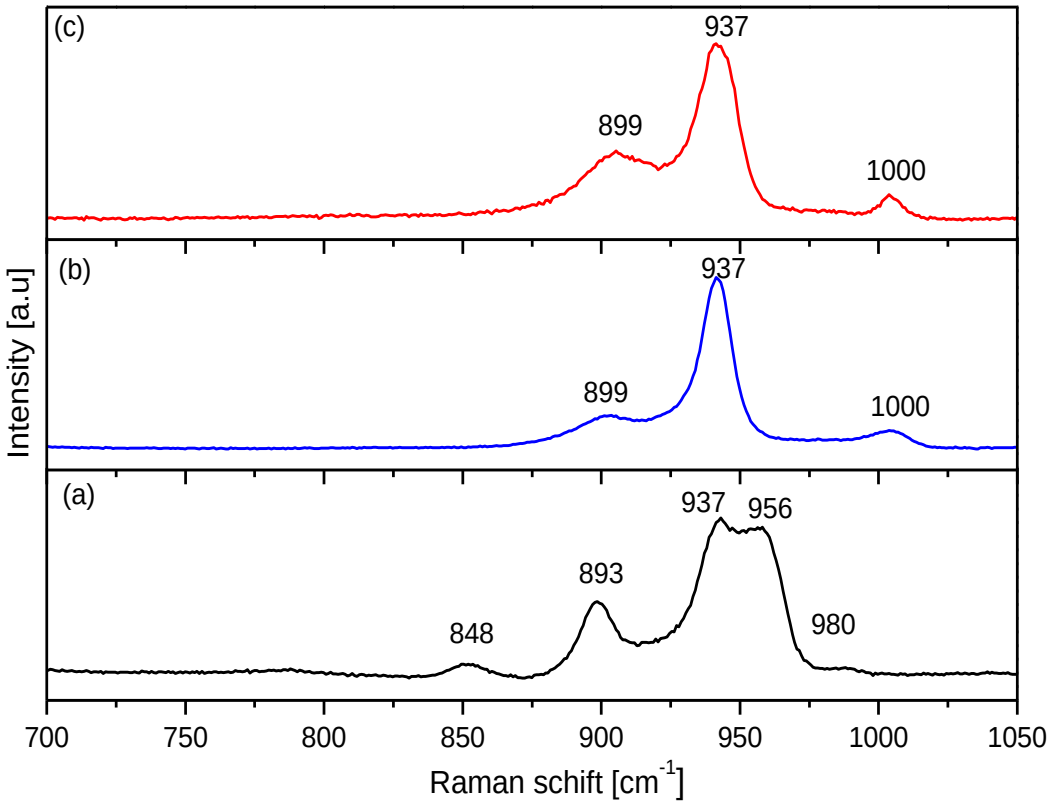

Figure 5.4: In-situ Raman spectra of (a) the binary MoV solution (pH=5.5, T= 353 K), (b) the ternary MoVTe solution (pH=5.0,T=353 K) and (c) the formation of MoVTeNb slurry

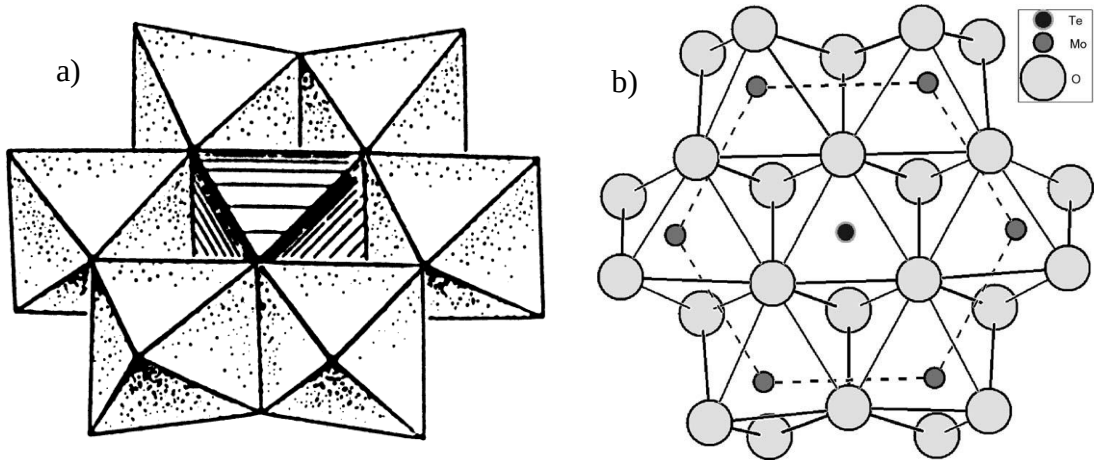

Figure 5.5: a) Structure of typical Anderson-type anion (Cabello, I.L.Botto et al. 2000) and; b) Schematic representation of Anderson-type anion (Beato, A. Blume et al. 2006).

According to Cobello and his group, the Anderson-type structure $[(Mo_6TeO_{24})^{6-}$ has a hexagonal plane structure composed with structural X ion which is surrounded by 6 octahedral MoO_6 groups. Each MoO_6 shares an edge with each of its two neighboring MoO_6 and another edge with the XO_6 or X $(OH)_6$ octahedron. This plane structure has the advantage of achieving good contact area/point with the support surface.

Yuhao et.al have synthesized a vanadium substituted heteropolytellurate $(NH_4)_7TeMo_5VO_{24}.8H_2O)$ (Yuhao, L.Jingfu et al. 1986). The replacement of one molybdenum atom in $(NH_4)_7TeMo_5VO_{24}.7H_2O$ by vanadium has shifted the stretching mode of the terminal M=O bonds from 946 to 990 cm^{-1}. This observation is identifiedin Fig. 5.4 (b), where molybdenum is partially replaced by vanadium in the formation of an Anderson-type heteropolytellurate phase. On the other hand, the band at 937 cm^{-1} which corresponds to the Anderson–type heteropolyanion also can also observed for heptamolybdate species. This implies that there is unconverted AHM remaining in the

ternary MoVTe solution. However, since the band at 644 cm^{-1} due to the hexaoxotelluric acid is no longer observed, a quantitative reaction of AHMand an additional incorporation of vanadium into the molybdotellurate seems to be highly probably, because the amount of tellurium added exceeds the Mo:Te stoichiometry in $[TeMo_6O_{24}]^{6-}$.(Beato, A. Blume et al. 2006).

Figure 5.6 shows the comparison of Raman spectra for ternary MoVTe solution and the spray dried precursors. When the strongly acidic niobium oxalate solution was added at 296 K into the ternary MoVTe, the pH dropped from 5.0 to 3.2 and accompanied by the formation of precipitate after the induction period in several seconds. The precipitate was aged for 60 minutes to become slurry. After spray-drying , fine orange powder was obtained. The samples before and after the addition of niobium oxalate solution were spray dried for structural comparison in the ternary MoVTe solution (Figure 5.6 (a) and 5.6 (b)). The band pattern of the both spray dried samples is retained but all the bands appear much broader after the addition of niobium oxalate solution.

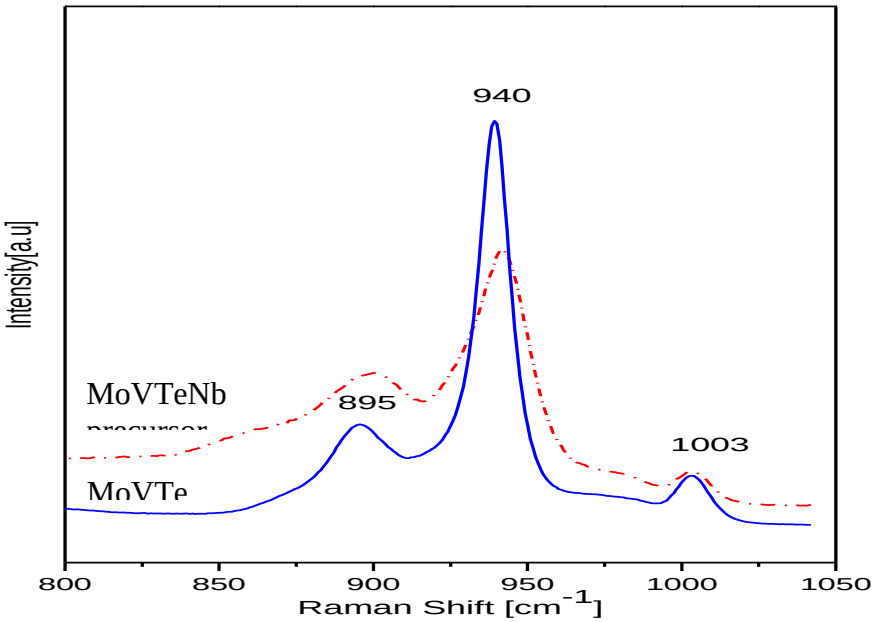

Figure 5.6: Raman spectra of the spray dried precursors (a) MoVTeNb and (b)MoVTe

5.1.3 Solidification/Drying

Highly dispersed nanostructured particles which can be prepared by precipitation method, followed by spray drying technique are found to exhibit high selectivity in propane oxidation to acrylic acid. These respective methods demonstrate prospective route for the synthesis development of mixed metal oxide catalyst. In fact, spray drying is an interesting method to exhibit the unique properties of catalyst and to improve the catalytic activity of a reaction. Drying is described as the elimination of water or any solvent from the pores of solid and it is often the second step involved in metal oxide preparation.

An effective MoVTeNb oxide catalyst for propane selective oxidation to acrylic acid can be obtained with the combination of proper preparation procedures and drying methods. In this study, the selected drying method is spray drying, which favors the formation of homogeneous dispersed of nanostructured particles. Spray drying involves evaporation of moisture from an atomized feed by mixing spray and drying medium. The typical drying medium is air. Different kinds of pressure can be used to disperse the liquid into fine particles. High pressure of air flow leads to high energy of dispersion. The higher the temperature is applied in the drying process, smaller droplets are generated. In general, the concept of spray drying involves the use of co-current flow in which the droplets come into contact with hot drying air in the same direction (see Figure 5.7).

1. Air inlet
2. Electric heater
3. Concentric inlet of the hot water around the spray dryer nozzle
4. Spray dryer cylinder
5. Cyclone to separate particles from gas stream
6. Collecting vessel of dried product
7. Outlet filter
8. Aspirator to pump air into system

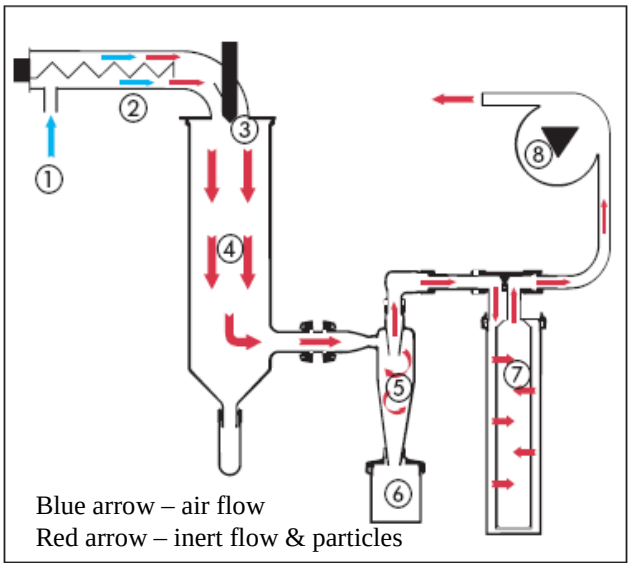

Figure 5.7: Functional principle of the spray drying technique

The slurry which obtained from the LabMax reactor was solidified with Büchi Mini Spray Dryer B-290 is show in Figure 5.8. The drying process can also be accompanied by physico-chemical and physico-mechanical transformations that can profoundly modify the structure of the gel. During this process, the constituent particles of a gel are subjected to a very large capillary tension which decreases as the diameter of the pores increases. This capillary force tends to bring the particles closer together, whereas both the chemical bonds binding the particles and sometimes the repulsions of electrostatic charges tend to maintain the structure. The optimization parameters of spray drying can be found in Appendix 1.

Figure 5.8: Mini Spray Dryer Büchi B-290

During spray drying, crystallization and a freezing-like process are competing. This type of solidification process is caused by the short residence time and therefore an abrupt removal of solvent. Some extreme case, the rate of (residence time of drying (t_{dry}) > crystallization rate (t_{cryst})). The other extreme case ((t_{dry}) < (t_{cryst})) applies when the crystallization rate is much faster than the drying process. In this case, well defined crystalline products with homogenous properties are obtained. In this respective catalyst system, drying process takes place on a faster time scale than a crystallization process. Therefore, the investigation conducted was based on the application of spray drying as a solid structure forming tool in which it is possible to accomplish better structural properties of the catalyst with reliable reproducibility.Thus, examinations by *Le et al.* on the Bi–Mo oxide catalyst system for selective propylene oxidation revealed that spray dried samples generally showed purer and homogenous sample properties with high reproducibility (Le, Craenenbroeck et al. 2003). The option to control the desired properties of the solid in a

narrow parameter range opens the door to the fundamental understanding of the ambiguities on the genesis of active and selective catalyst structures.

Figure 5.9 shows the formation of samples homogeneous orange fine powder from the spray drying. The particle size of the spray dried sample is in a broad range size which might due to the extreme heat treatment exerted on the sample which results in the difficulty to release the sudden steam produced. This consequently results in the formation of large beads. The anions and cations like oxalates and ammonium respectively tend to decompose because spray drying process was conducted in high temperature to form micro granules. This is proven by thesis Omar 2005, where higher temperature led to higher moisture diffusivity (Omar 2005). Prabhanjan *et.al.,* reported that higher drying temperature provides a larger water vapor pressure deficit or the difference between the saturated water vapor pressure and the partial pressure of water vapor in air at given temperature, which is one of the driving forces for catalyst drying (Prabhanjan, H.S. Ramaswamy et al. 1995).

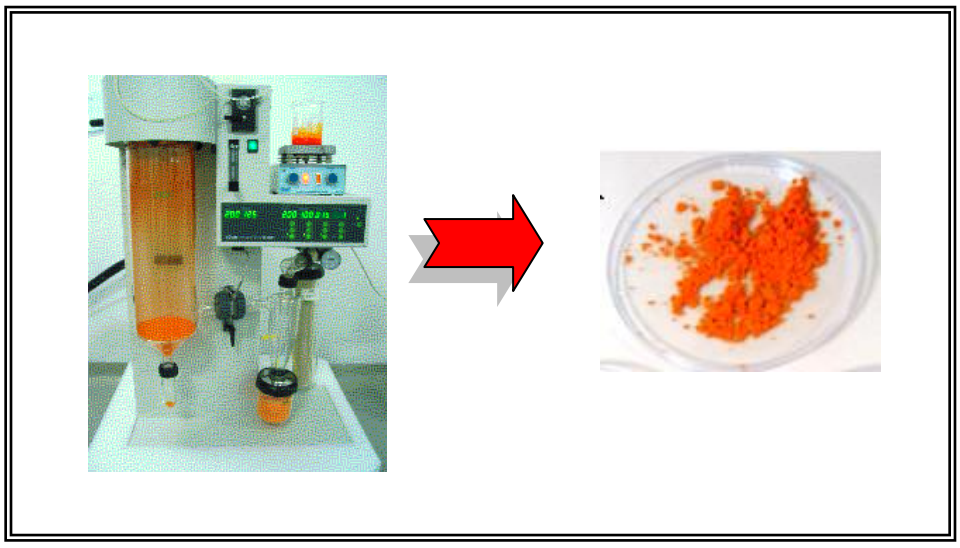

Figure 5.9: The formation of orange fine powder by mini spray drying unit.

The morphology of the prepared particles is mostly spherical, the presence of other morphologies such as needle-like and rod-like structures is also observed after the activation of the precursor.

5.1.4 Activation

Activation or calcination is defined as the process of subjecting a substance (precursor) to the action of heat without fusion, whereby causing some changes in physical or chemical properties. The purposes of calcination or activation process are usually: a) to drive off water, present as absorbed moisture, as “crystallization water,” or as “absorbed water” ; b) to drive off organic ligand or any volatile compounds; or c) to oxidize or reduce a part or the whole of compound (Lenntech 2007).

Calcination is typically the last step for the preparation of the oxide catalyst, where the composition and in particular, the bulk and surface structures of the oxides are finally settled, which ultimately determine the performance of the catalysts. Often, heating is done in the present in gaseous environment such as inert (flowing argon or helium) or reactive gas (flowing air, oxygen or hydrogen) in order to burn off any residual organics or to oxidize (or reduce) the sample. Exposing the sample to a high temperature over an extended period of time leads to sintering and consequently to a decrease in surface area. The process can also cause the material to crystallize into a different structural form or inactive oxide catalyst. Thus, the physical characteristics of a product depend on influencing parameters such as temperature, heating rate, time, and the nature and condition of the calcinations atmosphere (Ertl , H. *et al.* 1999). Calcination process is a decisive stage in dictating the structural properties of a catalyst as it creates porosity and texture via the lost of solvated molecules or

ligand to form the precursor and turn into active material. The new structure which is poorly organized, but becomes more organized and evolve into the final product with increasing temperature during calcination process. The activation of MoVTeNb precursor is accompanied by physico-chemical and physico-mechanical transformations which modify the structure of the solid from metastable phase to stable or crystalline structures such as Mo_5O_{14}-type or MoO_3.

As mentioned in the previous Chapter 3, the activation procedure of $Mo_1V_{0.3}Te_{0.23}Nb_{0.12}$ precursors involves two main steps. The first step is calcination where the precursor was calcined in synthetic air at 548 K (heating rate 10 K/min) and held for 1 h. The resulting material is designated as calcined material. In the second step,, the calcined material was heated from room temperature to 873 K with a rate of 2 K/min in argon. The final temperature was held for 2 h. The obtained material is designated as activated catalyst.

The procedure disclosed by Ushikubo *et.al.* for MoVTeNb oxide catalyst appears to be rather simple to implement. The precursors were calcined under an atmosphere of either N_2 or air at 600^{o}C for 2 h to produce the mixed metal oxide catalyst (Ushikubo, Nakamura et al. 1995). However, *Lin* found that the presence of air during the high temperatures calcinations, even at relatively small amount, is extremely detrimental to the effectiveness of the resulting MoVTeNb oxide catalyst. From his experiments, the results clearly show that the calcination atmosphere, whether in air or inert atmosphere (nitrogen or argon) plays a very critical role in the determination of the catalytic performance. Lin et.al reported that significant amount of MoO3 phase is formed in the MoVTeNb oxides when the calcination is conducted in air, and since it is known that pure MoO3 is inactive for the

selective oxidation of propane to acrylic acid (Lin 2003). Asakura *et.al* also reported that high activity catalysts could be obtained by calcination processes under an O_2-free atmosphere, or under N2 or He flows contaminated with less than 100 ppm of O_2. When there was more than 1000 ppm of O_2-contamination in the calcinations atmosphere, α-MoO_3 was found to form at the surface region, resulting in the reduction of the activity (Asakura K, Nakatani K *et al.* 2000).Therefore, calcination of MoVTeNb oxides conducted in air is not a recommended step due to formation of MoO_3.

Catalyst precursor also can be calcined in an oxidizing atmosphere at a lower temperature stage and non- oxidizing atmosphere at a high temperature stage. Argon is the best inert atmosphere for calcination in higher temperature than nitrogen or air. As an inert gas with higher density, argon offers better blanketing effect compared to nitrogen in an open calcination system to prevent air from contacting the samples in the bottom of calcinations containers. Manhua Lin has demonstrated several experiment to confirm the effect of calcinations atmosphere and successfully approved with argon give high catalytic performance (Lin M.M. 2003). In the experimental set-up, the catalyst precursor was placed in the crucible and the filled crucible was then placed in a covered stainless steel container called URN where the inert-flow was introduced from the inlet and outlet of the container. The color comparison of the sample before and after activation process is shown in Figure 5.10.

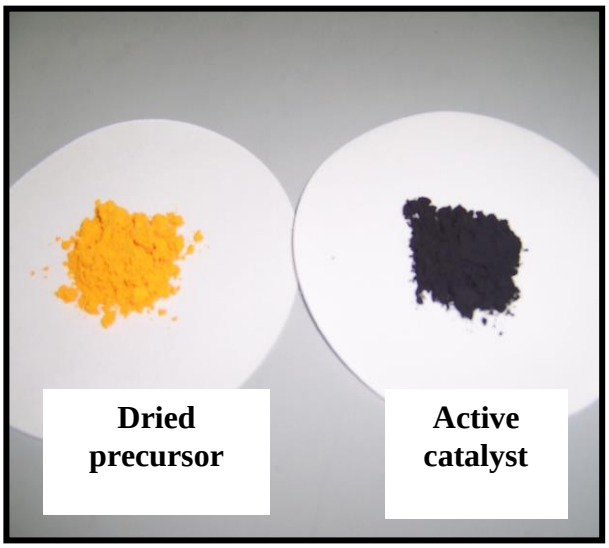

Figure 5.10: Orange fine powder (MoVTeNb precursor) and black fine powder (MoVTeNb oxide catalyst)

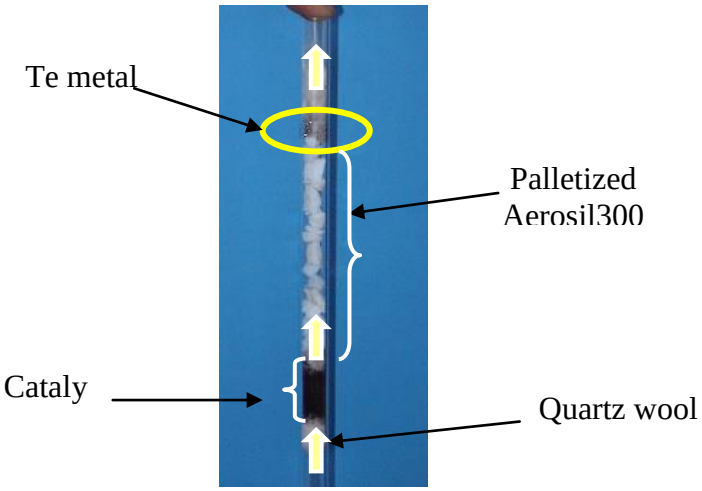

Figure 5.11: Experiment of evidence on Te evaporation during calcinations in inert atmosphere at 898 K.

Evaporation of metallic Te from the bulk of MoVTeNb oxide during calciantion is lead to the poor selectivites of acrylic acid. According to Lin *et.al*, this significant lower acrylic acid selectivity as a result of Te loss is very consistent with the previous discussion that Te are believed to be closely involved in the active phase responsible for the formation and or the release of acrylic acid form the catalyst [Lin *et.al* , 2003]. The melting point of Te is

approximately 723-748 K where Te was decomposed, likely in a vapor form from the bulk MoVTeNb oxide catalyst during calcination process. In order to prove that the Te component in the catalyst system is decomposed in metallic Te form during calcination process, a small amount (~ 1g) of MoVTeNb oxide catalyst was loaded in a quartz tube with palleted aerosil 300 placed on top of the catalyst (Figure 5.11). The catalyst and the aerosil 300 were separated by quartz wool. The calcination was carried out at 898 K for 2 hours in flowing of He gas (heating rate 10K/min). It could be clearly seen that a significant amount of Te metal was deposited at the top of the gas-vent of the calcinations device after the calcination process. At about 898 K under the inert atmosphere, the reduction of Te ion to Te metal was likely to take place and subsequently, the gas-flow carries the metallic Te^0 vapor from the surface of the catalyst The loss of Te can be avoided if a suitable oxygen partial pressure is maintained in the main calcination phase over the decomposing of Te-acid or Te-O_2. This is not possible in the presence of organic reducing species as these species can lead to the thermal decomposition of Te compounds leaving behind sub-oxides and metallic Te.

5.2 Catalyst Characterization

The physical and chemical characteristics which are commonly studied for solid materials are crystallinity, elemental composition, surface area, porosity and reactivity in probing reactions. In order to perceive the physical and chemical properties, the prepared catalysts were characterized using numerous techniques as discussed in Chapter 3. The composition and structural analysis in this work were studied by using XRD, SEM/EDX, XRF and FTIR while the thermal behavior was investigated by TGA, DSC and TPR techniques.The prepared samples are listed in Table 5.3.

Table 5.3: Lists of sample prepared

Catalysts Code	Composition	Calcination Temperature (K)		Category
		Calcined	**Heat-treatment**	
A1	Undiluted $Mo_1V_{0.3}Te_{0.23}Nb_{0.12}$	548 in air	873 in argon	**Standard Method (Reference catalyst)**
A2	Undiluted $Mo_1V_{0.3}Te_{0.23}Nb_{0.12}$			**Modification 1: Addition of oxalic acid**
B1	Diluted $Mo_1V_{0.3}Te_{0.23}Nb_{0.12}$	598 in air	923 in argon	**Standard Method (Reference catalyst)**
B2	Diluted $Mo_1V_{0.3}Te_{0.23}Nb_{0.12}$			**Modification 2: Addition of oxalic acid**

5.2.1 XRD

The bulk crystalline phase of the as-prepared catalysts was determined by X-ray diffraction analyses. It has been proved that the dried precursor exhibit poorly crystalline phases. The crystallization only occurs after the calcinations process (Lin M.M. 2003). It is known that a good catalyst for oxidation of propane to acrylic acid should be a mixture of orthorhombic and hexagonal phases of MoVTeNb system which can be referred as M1 and M2 phases respectively. In addition, a third phase which is known as 'Anderson Mo-tellurate' crystallized in rutile and triclinic variants can also be present. The structural arrangement of the material and the existence of many different Mo-O bond lengths are the vital cause for the high catalytic performance of the catalyst.

It has been recently reported that both M1 and M2 phases involved in the selective ammoxidation of propane with M1 showing high conversion rates of propane and M2 showing higher selectivity to acrylonitrile. The key relevance for this contribution is the ortho phase. Without its presence, there is little catalytic activity in propane to acrylic acid

conversion. It is also noted that the structure of Mo_5O_{14} is very similar to the M1 structure, as both of them contain pentagonal bypyramides and hexagonal channels (Knobl, Zenkovets et al. 2003).

The M1 phase was identified by the major XRD reflections at 2θ ° of 6.6°, 7.8°, 9.0°, 13.0°, 22.1°, 26.2°, 26.8°, 27.6° and 45.2°, while the M2 phase was characterized by the major reflections at 22.1°, 28.3°, 36.2° and 44.6° (Ushikubo, Oshima et al. 1997; Aouine, Dubois et al. 2001; Oshihara, Hisano et al. 2001; Al-Saeedi, Vasudevan et al. 2003; DeSanto, Buttrey et al. 2003; Grasselli, Burrington J.D. et al. 2003; Vitry, Morikawa et al. 2003). Although a significant overlap of the XRD reflections is observed for these two phases, the M1 phase may be detected by the presence of reflections at $2\theta < 10^o$, while the presence of the M2 phase is manifested in the characteristic reflection at $2\theta = 28.3^o$ (Guliants, Bhandari et al. 2004). In this study, the XRD reflections observed were compared to the simulation data of M1 and M2 phases. The simulation is based on data published by DeSanto et. al. (DeSanto, Buttrey et al. 2003).The lattice parameters were adjusted slightly to yield a better match of the peak positions. A quantitative analysis was further attempted by using Bruker TOPAS software. Rietveld refinement on the catalysts was performed using crystal model proposed by Grasselli et. al.

The $Mo_1V_{0.3}Te_{0.23}Nb_{0.125}$ oxide catalyst was prepared as a reference for both undiluted and diluted system (Table 5.3). From the screening work discussed in Chapter 4, the addition of silica has improved the catalytic performance. On the other hand, , silica was added as a diluent to the solution in the synthesis with the aim to separate the individual crystallites of

the phases in such a way that sintering or Ostwald ripening of nanostructures is minimized under the harsh reaction conditions (Wagner, Timpe.O. et al. 2006).

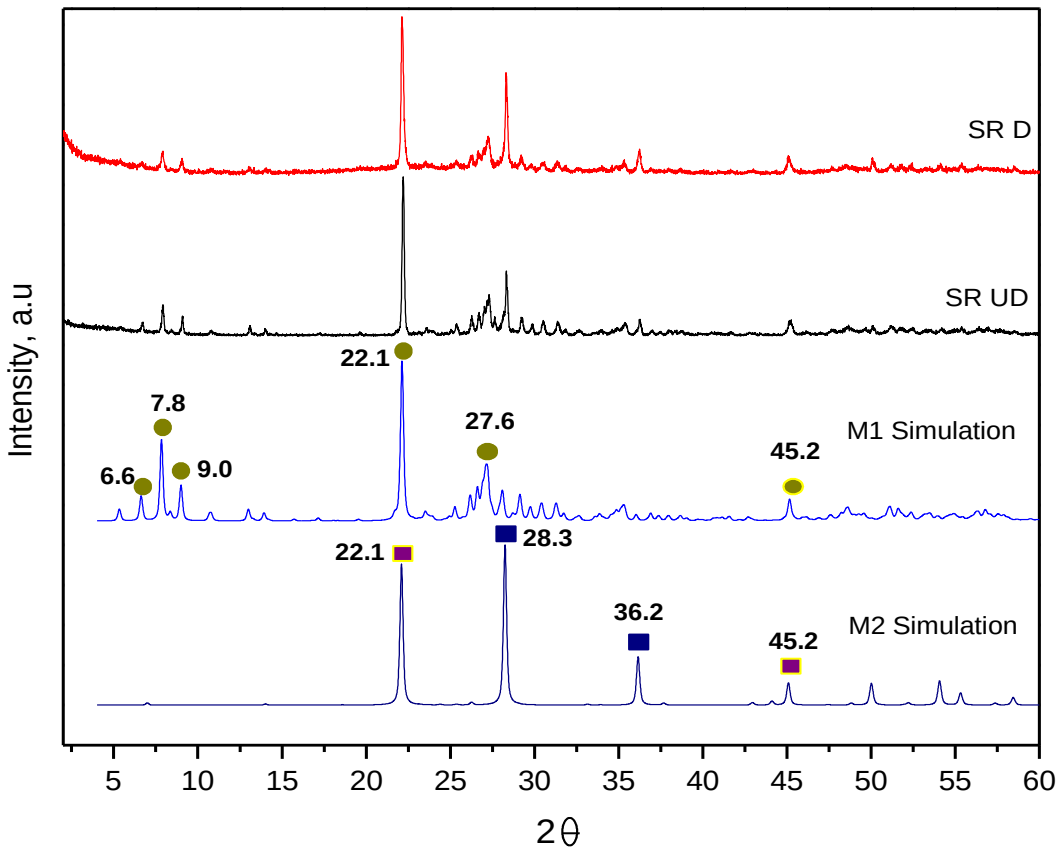

Figure 5.12: X-Ray diffraction patterns of standard recipe for undiluted (SR UD) and diluted (SR D) $Mo_1V_{0.3}Te_{0.23}Nb_{0.12}$ with reference to M1 and M2 phase simulation.

Figure 5.12 has shown the diffraction pattern for undiluted and diluted MoVTeNbOx catalyst. The M1 and M2 phases were observed in both systems. Both systems showed similar reflections. Three identical peaks arose at $2\theta < 10^{o}$ although the intensity of these two catalyst is comparatively lowered as compared to the simulation data.

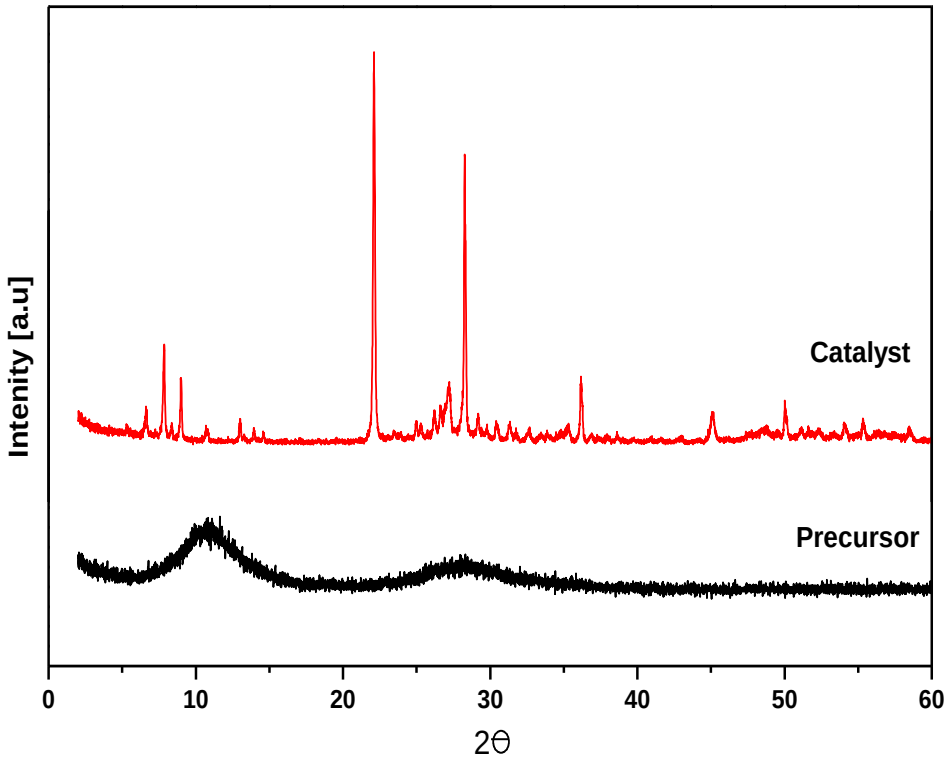

Figure 5.13: X-ray diffraction pattern for precursor and activated $Mo_1V_{0.3}Te_{0.23}Nb_{0.125}$ oxide catalyst.

The diffractograms of dried and activated/calcined $Mo_1V_{0.3}Te_{0.23}Nb_{0.125}Ox$ are illustrated in Fig. 5.13.The diffractograms reflect the changes in crystal phases as a result of crystal structure rearrangement after calcination process. The significant crystal phase transformation of this system reveals that the drying technique applied herein affects the structural formation of a catalyst and this in turn affects the catalytic performance.

The spray dried precursor is X-ray amorphous as it shows relatively broad peaks in the pattern. These broad features are found at 2θ = 11°, 27° and 34°which resemble the intensity distribution of reflections for the crystalline Anderson-type heteropolyanion $(NH_4)_6[TeMo_6O_{26}]\cdot 7H_2O$ (Evans Jr. 1968). One reason for this broad signal might be that the degree of polymerization due to condensation in water at the chosen conditions is too low to form big crystalline particles or the solubility of the product has reached too early. DSC and TG-MS clearly show that there is an on-going polycondensation. This observation is in line with the Raman spectroscopic results with the presence of Anderson-type anion in the spray dried precursor. Thus, it could be seen that no significant changes occur in the local arrangement during the slurry formation and spray-drying process as compared with the pre-assembled structures in solution.

i) Undiluted system

The effect of reductive oxalic acid in preparation of precursor and standard MoVTeNb precursor can be seen in Figure 5.14. Catalyst A2 is modified by adding reductive oxalic acid during preparation. In fact, the presence of reducing agent during the MoVTeNbO catalysts preparation by hydrothermal or slurry methods strongly influences both nature of crystalline phases and catalytic activity (Grasselli, Burrington J.D. et al. 2003; Oliver, López Nieto et al. 2004; Botella, Concepción et al. 2005; Solsona, Vázquez et al. 2007). Much attention was focused on the study of the structure and chemical composition of the phases M1 and M2 and the oxidation states of their constituent elements (Asakura, Nakatani et al. 2000; Zhonghua, Hongxin et al. 2008; Yi, Sun et al. 2009). Figure 5.14 shows that both diffractograms for catalyst A1 and catalyst A2 presents M1 and M2 pahses exists in the system. The appearance of peaks at 2θ = 6.6°, 7.8°, 9.0°, 22.1°, 27.6°, 28.3° and

36.2^{o} can mainly be related to an orthorhombic $Te_2M_{20}O_{57}$ (M=Mo, V and Nb) phase (Millet, Roussel et al. 2002). In addition, peaks at 2θ = 22.1^{o}, 28.2^{o}, 36.2^{o} and 45.2^{o} and 50.0^{o} can be related to $Te_{0.33}MO_{3.33}$ (M = Mo, V, Nb) which is a crystalline phase with its XRD pattern similar to that of a hexagonal tungsten bronze ($K_{0.13-0.33}WO_3$, HTB) (Botella, López Nieto et al. 2002; Garcia-Gonzalez, Lopez Nieto et al. 2002; Millet, Roussel et al. 2002). It has been known (Ushikubu T, Oshima K et al. 1997; Lin 1999) that the effective MoVTeNbO catalyst for the selective oxidation of propane to acrylic acid should have peaks at diffraction angles of 2θ = 22.1^{o}, 28.1^{o},36.2^{o},45.1^{o} and 50.0^{o}. The orthorhombic phase M1 has characteristic peaks with 2 θ at 22.1 ^{o} and 45.1 $^{o.}$ The pseudo hexagonal phase M2 has characteristic phase with 2 θ at 28.3 ^{o}, 36.4 ^{o} and 50.3 ^{o} (Yu, Zheng et al. 2011).Apparently, all the five characteristic peaks of M1 and M2 phases exist in the sample which indicates that an effective catalyst is successfully formed.

By matching the sample's diffractogram with the reference in EVA software, the peak at 2θ= 22.1^{o} (M1 phase) can be related to the presence of several Mo-containing phases i.e., $(V_{0.07}Mo_{0.93})_5O_{14}$ (peaks at 2θ = 16.5 ^{o},22.3 ^{o}, 23.3 ^{o}, 24.9 ^{o},28.2 ^{o}, 31.5 ^{o} and 33.7 ^{o})(PDF No: 31-1437), $(Nb_{0.09}Mo_{0.91})O_{.2.8}$ (peaks at 2θ = 16.5 ^{o}, 22.1 ^{o}, 23.2 ^{o}, 24.9 ^{o}, 26.1 ^{o},27.6 ^{o},28.1 ^{o},31.3 ^{o}, 31.5 ^{o}, 32.4 ^{o} and 33.5 ^{o}) (PDF No: 27-1310), MoO_3 (peaks at 2θ = 12.7 ^{o},23.3 ^{o},25.6 ^{o},27.3 ^{o}, and 38.9 ^{o}) (PDF No: 05-0508), $TeMo_5O_{16}$ (PDF: 31-0874) and/or $TeMo_4O_{13}$ (PDF No: 34-0622) (peaks at 2θ = 21.7^{o}, 24.6 ^{o}, 26.2 ^{o}, 26.7 ^{o},30.5 ^{o} and 34.9^{o}).

The peak at 2θ = 28.2 (M2 phase) can be related to $(V_{0.07}Mo_{0.93})_5O_{14}$, $(Nb_{0.09}Mo_{0.91})O_{2.8}$ and $Te_4Nb_2O_{13}$ (peaks at 2θ = 23.5 ^{o}, 24.9 ^{o}, 27.2 ^{o}, 28.0 ^{o}, 31.6 ^{o}and 37.2 ^{o}) (PDF No: 36-1175). In recent published literature (Botella, López Nieto et al. 2002), the five

characteristic peaks at 2θ = 22.1 °,28.2 °,36.2 °, 45.1 ° and 50.0 ° were assigned to a new TeMO (TeVMoO or TeVNbMoO; M= Mo,V,Nb) crystalline phase. Aouine and his group considered that the new TeMO crystalline phase could correspond to the phase $Te_{0.33}MO_3$ (M= Mo,V and Nb). While Baca and his co-workers considered that the new TeMO crystalline phase could be related to two major phases M1 $[(Te_2O)M_{20}O_{56}]$ and M2 $[(TeO)M_3O_9]$ (M=Mo,V) having orthorhombic and hexagonal structure, respectively, and the orthorhombic M1 phase is found to be the most active and selective phase for propane oxidation, a synergism effect between M1 and M2 phases which improves the catalyst performances.

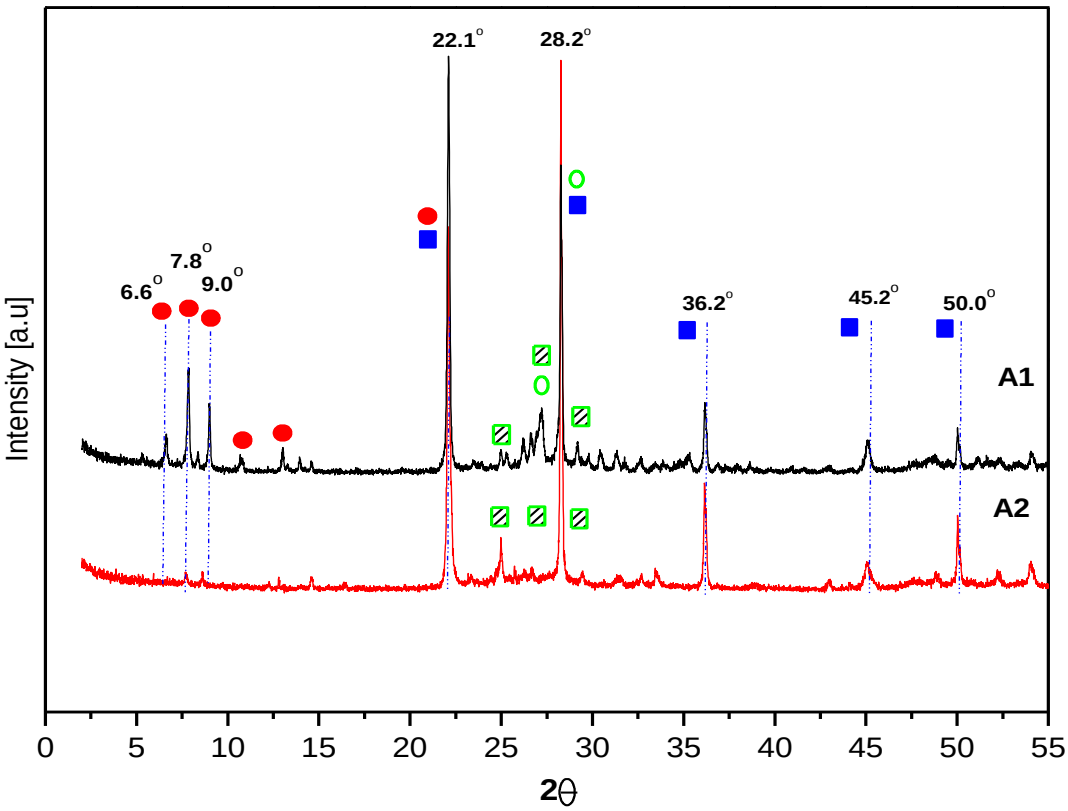

Figure 5.14: XRD patterns for catalyst A1 (standard sample) and catalyst A2 (addition of oxalic acid) of the MoVTeNbO catalyst with reference peaks: ( ) M1 Phase or $Te_2Mo_{20}O_{57}$, ( ) M2 phase or $Te_{0.33}MO_{3.33}$, ( ) MoO_3 and ( ) $TeMo_5O_{16}$

Table 5.4: Phase composition compared to catalytic performance in undiluted MoVTeNb oxide system

Catalyst ID	Rieveld refinement (%)		Catalytic Performances (%)		
	M1 (%)	M2 (%)	C3 conversion	AA selectivity	AA yield
Catalyst A1	50.61	49.39	8	41	3
Catalyst A2	58.53	41.47	39	51	19

Table 5.4 shows the relative percentage of M1 and M2 phases in the MoVTeNb oxide catalyst which was calculated using *Rietveld* refinement method (Refer Appendix). From the table, A1 catalyst gives approximately 50:50 of M1 to M2 phase Addition of oxalic acid in A2 catalyst increases the concentration of M1 phase to nearly 60% in comparison to 40% of M2 phase. This observation of amorphous and M1 and M2 crystalline phases are also confirmed by TEM analysis for standard MoVTeNb oxide catalyst (see Figure 5.15) where spray dried sample consists of well crystalline particles with particle size of 100 nm All the lattice fringes fit very well to the M1 phase while some parts of the images fit M2 phase as well. The amorphous layer can be found at the edge of crystalline phase. The XRD results show that the addition of oxalic acid leads to the change of the phase composition whereby achieving 39% conversion, 51% selectivity and 19% yield of acrylic acid. The addition of oxalic acid affects the phase composition of M1 and M2 phase in the catalyst system. According to the XRD results, the amount of M1 phase in the catalyst system can only be increased in the presence of oxalic acid by employing slurry method. It is evident that the addition of right element can greatly enhance the catalyst system which results in good catalytic performance.

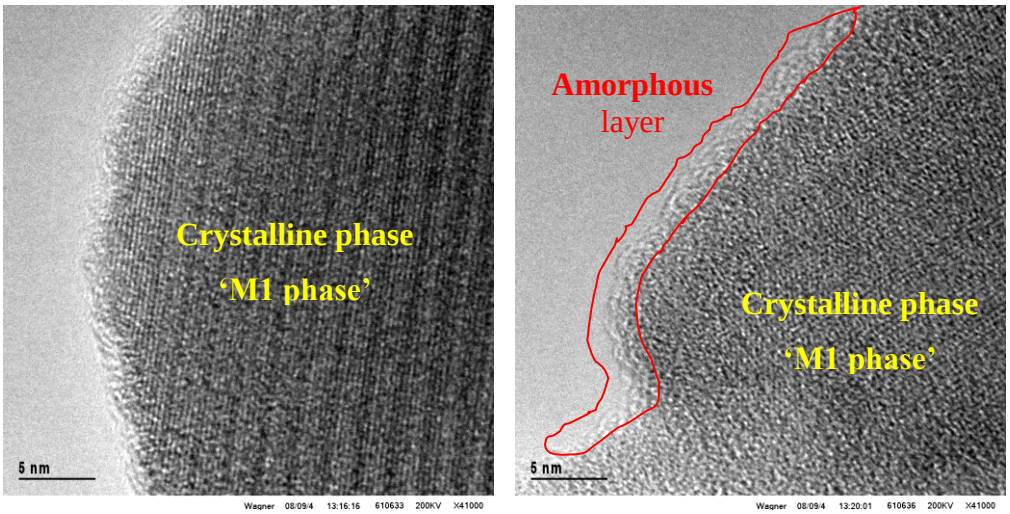

Figure 5.15: The crystalline and amorphous phases in TEM images for standard MoVTeNb oxide catalyst.

ii) Diluted System

There are two phases being identified to be present in the MoVTeNb oxide catalyst. The orthorhombic phase (denoted as M1) is responsible for propane activation and propylene formation, whereas the hexagonal phase (denoted as M2) is active and selective for acrylic acid generation. The XRD patterns for diluted system are shown in Figure 5.15. The XRD patterns at low diffraction angle ($2\theta < 10$) show that both of the undiluted and diluted systems show almost similar XRD patterns except that the catalyst with diluents is more crystalline than the undiluted system.. The reflections of silica are hardly spotted in the diffractogram due to its amorphous nature.

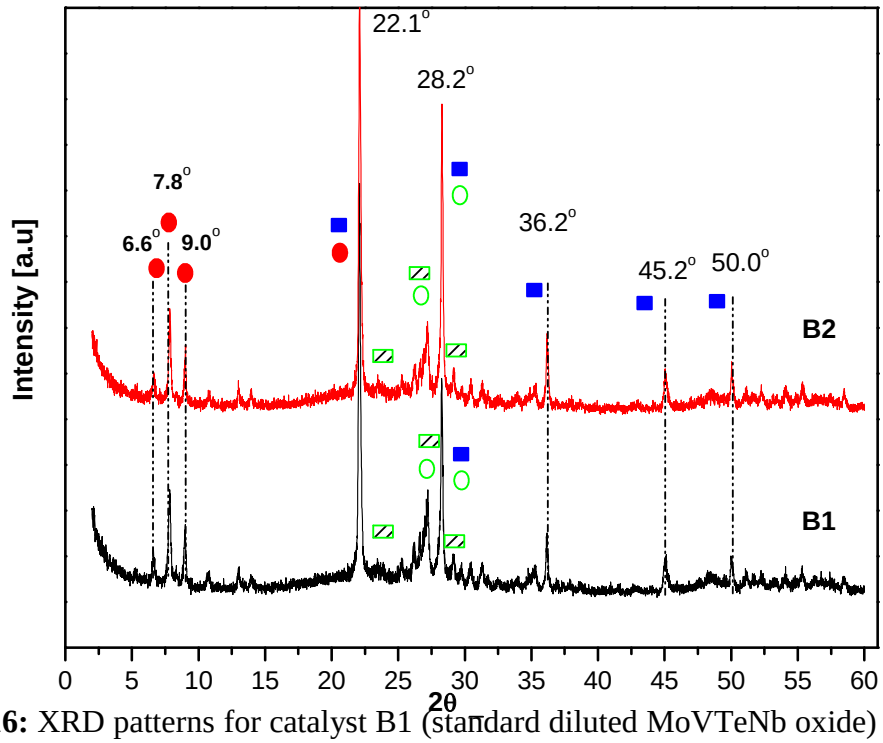

Figure 5.16: XRD patterns for catalyst B1 (standard diluted MoVTeNb oxide) and catalyst B2 (diluted MoVTeNb oxide with oxalic acid) with reference peaks: ( ) M1 phase or $Te_2Mo_{20}O_{57}$, ( ) M2 phase or $Te_{0.33}MO_{3.33}$, ( ) MoO_3 and ( ) $TeMo_5O_{16}$

In the diluted system, M1 and M2 phases can be identified from XRD diffractogram in Figure 5.16. The peaks at 2θ = 6.6°, 7.8°, 9.0°, 22.1°, 27.6°, 28.3° and 36.2° can be related to an orthorhombic $Te_2M_{20}O_{57}$ (M=Mo, V and Nb) phase (Millet, Roussel et al. 2002). Meanwhile, the additional peaks at 2θ = 22.1°, 28.2°, 36.2° and 45.2° and 50.0° can be related to $Te_{0.33}MO_{3.33}$ (M = Mo, V, Nb), a crystalline phase with XRD pattern similar to that of a hexagonal tungsten bronze ($K_{0.13-0.33}WO_3$, HTB) (Botella, López Nieto et al. 2002; Garcia-Gonzalez, Lopez Nieto et al. 2002; Millet, Roussel et al. 2002). Catalyst B2 show the distribution of M1 phase very high after addition of oxalic acid into the sample and composition of catalyst B1 and B2 can be seen in Table 5.5. In this case, the catalytic performance also increase where the conversion for B2 catalyst is slightly increased as compared to B1 catalyst. Addition of oxalic acid into the diluted system has greatly improved the activity of the catalyst. On the other hand, the catalysts B2 show high in

propane conversion but the selectivity to acrylic acid is remains the same. It could be due to formation of Cox during the reaction. No significant effect of reductive agents for diluted MoVTeNb oxide catalyst towards acryic acid production.

Table 5.5: Phase composition compared to catalytic performance in diluted MoVTeNb oxide system

Catalyst ID	***Composition percentage***		**Catalytic Performances (%)**		
	M1 (%)	**M2 (%)**	C3 conversion	AA selectivity	AA yield
Catalyst B1	54.42	45.58	30	76	21
Catalyst B2	66.91	33.09	38	76	29

The effect of activation is crucial to produce a good catalyst. Two steps calcination under air at low temperature followed by Argon in high temperature. Calcination under Argon can prevent the formation of MoO_3,which is non-selective in converting propane to acrylic acid. It can be concluded that drying and activation are the crucial parameters for establishing the catalyst structural reactivity relationship.

5.2.2 Micromorphology and Elemental Composition by SEM/EDX

Scanning Electron Microscopy is used to study the morphology and localized elemental composition of the materials. The morphology and localized composition of the dried precursor and final catalyst which has been calcined ($Mo_1V_{0.3}Te_{0.23}Nb_{0.125}Ox$) are displayed in Figure 5.17.

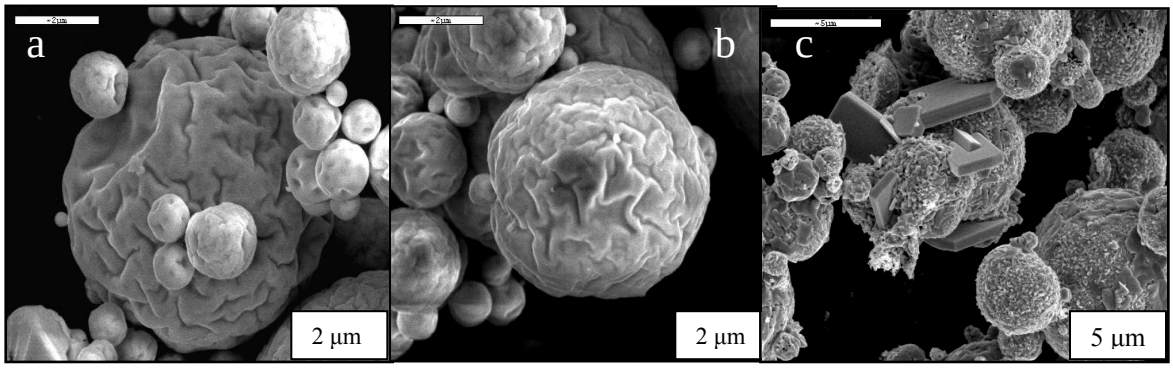

Figure 5.17: Typical SEM images of the spray-dried MoVTeNb undiluted system, (a) MoVTeNb dried precursor (b) dried precursor after calcined at 548 K in air and (c) After heat treatment at 873 K in Argon

The SEM images show the morphology of the catalyst after calcined in air at 548 K and heat treatment in Argon at 873 K for undiluted system whereas for diluted system the catalysts was calcined in air at 598 K and heat treatment in Argon at 923 K. The SEM images depict the morphology of the dried precursor of Mo-V-Te-Nb system (which is XRD amorphous). The sample consists mainly in a sphere shape with an uneven surface which consists of many dents resulted from drying process. The diameter of the mostly hollow particles varies between 1 to 40 μm. The shape and the size of the spherical particles do not change after calcination in air at 548 K (Figure 5.17b). The morphology of the sample has changed after heating at 873 K in Argon (Figure 5.74c). The spherical balls have different size of smaller particles with regular shape with diameter about 1 to 12 μm.

i) Undiluted System

The morphology of the MoVTeNb catalyst is known to be the critical property in determining the selective oxidation of propane to acrylic acid. Therefore, the SEM technique is used to study the texture and morphology of the reference and modified samples. EDX technique further identifies the surface chemical nature of mesoscopic objects. With electron microscopy alone it is also difficult to find the typical structure of a complex material.

Standard Recipe

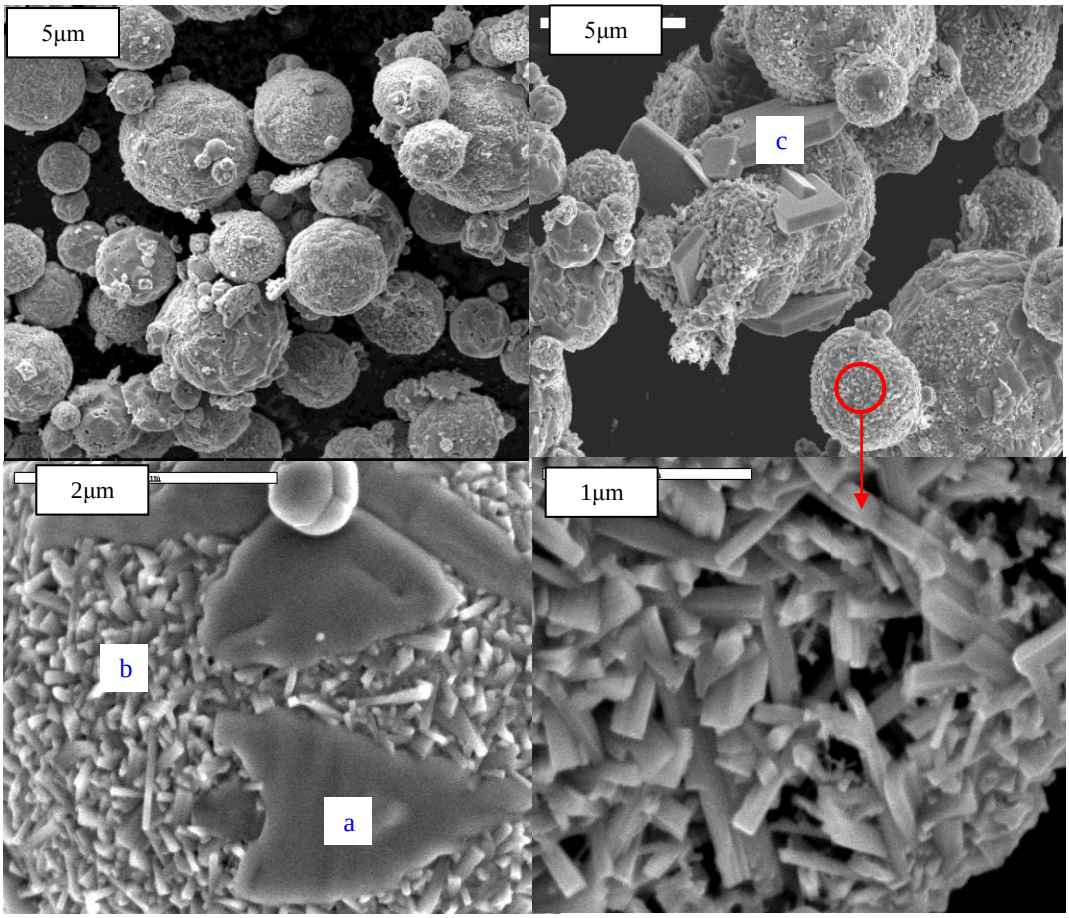

Elements	Normalized to Mo			
	theory	spot a	spot b	spot c
Mo	1.000	1.000	1.000	1.000
V	0.300	0.254	0.280	0.323
Te	0.230	0.109	0.221	0.346
Nb	0.125	0.191	0.027	0.082

Figure 5.18: SEM-images and EDX of undiluted $Mo_1V_{0.3}Te_{0.23}Nb_{0.125}Ox$ catalyst system after activation

Undiluted with oxalic acid

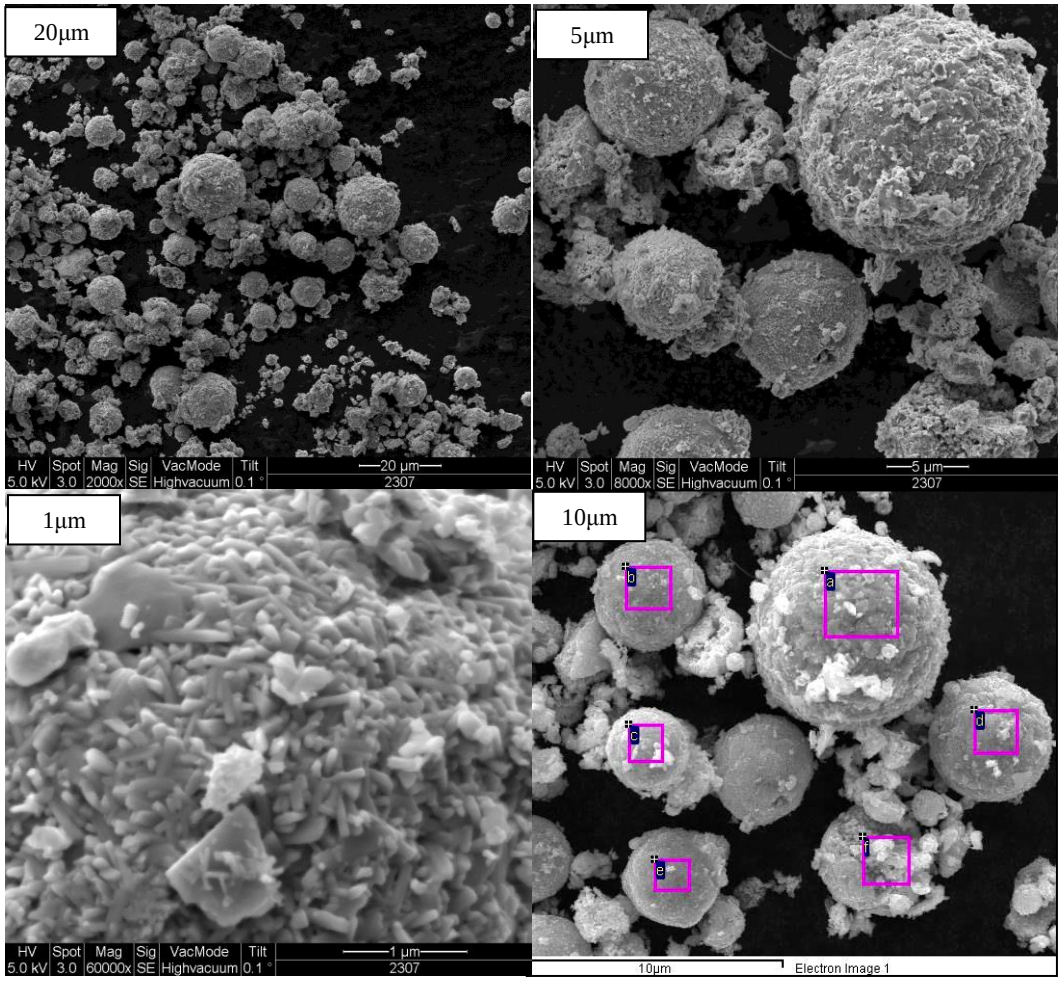

Element	Normalized to Mo						
	Theory	Spot a	Spot b	Spot c	Spot d	Spot e	Spot f
Mo	1	1	1	1	1	1	1
V	0.3	0.27	0.25	0.23	0.24	0.26	0.28
Te	0.23	0.19	0.16	0.14	0.18	0.11	0.12
Nb	0.125	0.120	0.160	0.240	0.120	0.160	0.140

Figure 5.19: SEM-images and EDX of undiluted $Mo_1V_{0.3}Te_{0.23}Nb_{0.125}Ox$ with oxalic acid after activation

The SEM-EDX analysis has revealed the multi-phase nature of the MoVTeNb oxide catalysts. A strong interaction among AHM, AMT, Te-acid and ANO ions resulting in the formation of Me-O-Me bridges and a mixed Mo, V, Te and Nb compound was observed with a structure closely related to the Mo_5O_{14}-type. This morphology was maintained during the spray-drying process but in XRD analysis shows amorphous structure. Further thermal treatment removed ammonia, water and oxalate and increased the crystallinity of the catalyst system.

The standard catalyst after activated in Argon has shown in Figure 5.17 (c). It is clearly shown that the spherical balls consists of agglomeration of rod-like particle which is believed to be an active site for MoVTeNb oxide catalyst. Some of the particles coated with plain surface and there is also big rod-like shape particles agglomerated in between of round particles. However, the EDX reveals inhomogeneous elemental distribution for the mentioned catalyst (Table EDX in Figure 5.17). Some areas of the particles are coated with small crystal, which are deprived of tellurium and vanadium. These small crystals possess a chemical composition closer to that M1 phase which is believed to be the active phase in propane oxidation to acrylic acid. Particle in spot b shows that area of the spherical

particle which is covered with other “molten” particles. From EDX analysis, this area showed an elemental composition which is closely resembled to M2 phase whereby Mo and Nb exhibits higher composition in relative to other elements. Nevertheless, the rod-like shaped particles are found to constitute higher amount of tellurium. This particle is suitable for total oxidation whereby further experiment proved that some of Te will evaporate during activation.

Figure 5.19 shows the images for undiluted MoVTeNb oxide catalyst with addition of oxalic acid. The morphology of this sample is also found to be in spherical shape. All the spherical particles are coated with agglomerated of small crystals. Furthermore, the EDX reveals homogeneous elemental distribution in each spots. Each spot shows lower Te content and some areas have higher amount of Nb. The addition of oxalic acid could give some effect of the morphology and the activity of the catalyst. It has been proven that by increasing the BET surface area of from 3.3 to 5.9 m^2/g, the conversion of propane can also be increased from 8 to 19%. All the composition distribution indicates that some of the variable admixtures gave additional abundance of molybdenum-vanadium ratios.

ii) Diluted System

Standard Recipe

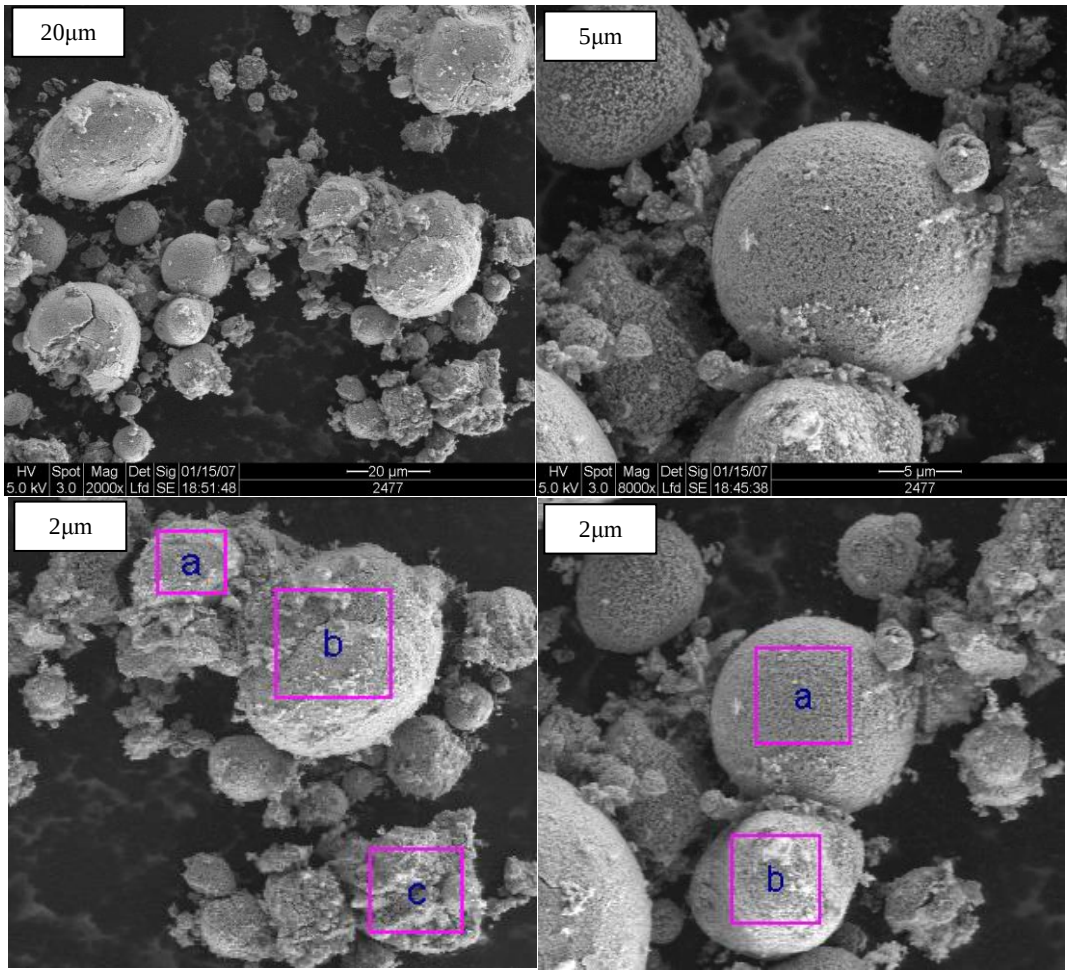

(i)

Elements	Normalized to Mo			
	theory	spot a	spot b	spot c
Mo	1.000	1.000	1.000	1.000
V	0.300	0.316	0.337	0.362
Te	0.230	0.254	0.261	0.224
Nb	0.125	0.126	0.113	0.113
Si	-	3.368	2.663	3.345

(ii)

Elements	Normalized to Mo		
	theory	spot a	spot b
Mo	1.000	1.000	1.000
V	0.300	0.284	0.273
Te	0.230	0.198	0.178
Nb	0.125	0.116	0.085
Si	-	2.752	2.434

Figure 5.20: SEM-images and EDX of the diluted $Mo_1V_{0.3}Te_{0.23}Nb_{0.125}Ox$ without oxalic acid after activation

Diluted system with oxalic acid

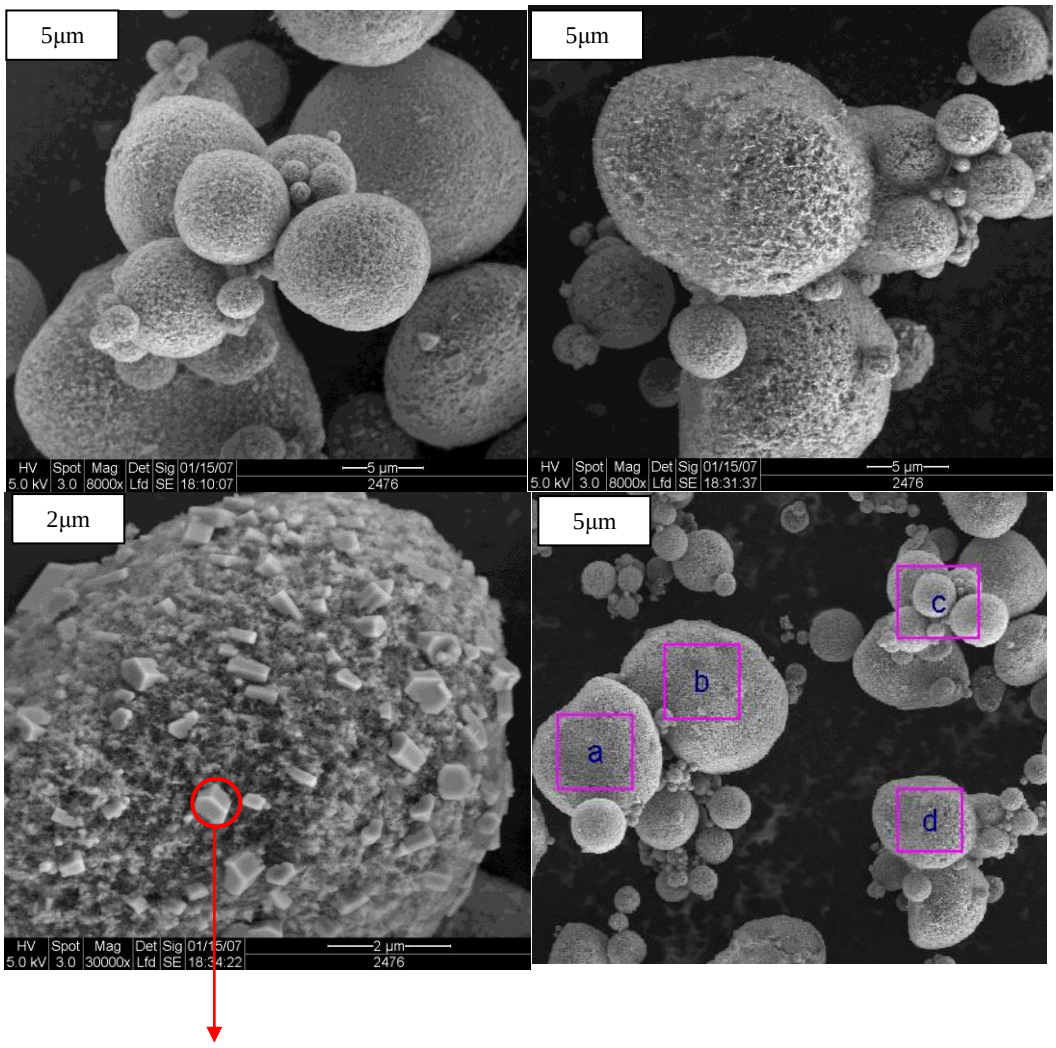

(i)

Elements	Normalized to Mo	
	theory	crystal
Mo	1.000	1.000
V	0.300	0.380
Te	0.230	0.275
Nb	0.125	0.062
Si	-	3.175

(ii)

Elements	Normalized to Mo				
	theory	spot a	spot b	spot c	spot d
Mo	1.000	1.000	1.000	1.000	1.000
V	0.300	0.235	0.334	0.212	0.354
Te	0.230	0.227	0.257	0.102	0.099
Nb	0.125	0.056	0.037	0.094	0.075
Si	-	2.219	2.167	3.997	2.467

Figure 5.21: SEM-images and EDX of the diluted $Mo_1V_{0.3}Te_{0.23}Nb_{0.125}Ox$ with oxalic acid after activation

In the diluted system (Figures 5.20 and 5.21), it was found that the spheres structure of the precursor which was formed during spray drying process are still remained after activation as shown in all the SEM images. The BET measurement revealed that the surface area and the porosity of the catalysts have been improved after the dispersion of the silica. The addition of oxalic acid does not alter the morphology of the catalyst. All catalyst showed particles which are enriched with Mo and V as well as low amount of Te as Te is evaporated during activation. The EDX of each sample shows homogeneity in the elemental distribution.

5.2.3 X-ray Fluorescence (XRF)

X-Ray Fluorescence is a spectroscopic technique of analysis based on the fluorescence of atom in X-ray domain, to provide qualitative and quantitative information on the elemental composition of a sample. Basically, it is used to measure the bulk composition of the element in the samples. All the related methods should be covered under Chapter 3, Research Methodology!) Tables 5.6 and 5.7 show the theoretical and experimental composition of MoVTeNb oxide catalyst by XRF analysis. The data in the tables tabulates the composition of metals in the catalysts which are normalized to Mo metal.

Based on the XRF result, the molar ratio for both undiluted sample revealed less amount of Te due to the decomposition of Te during activation. The distribution of elements for both samples is not much different. The addition of oxalic acid seems to increase the metal ratio of Nb and V as well. For diluted system, the elemental distribution for both samples is almost similar. However, the amount of Te has been decreased for both samples (as compared to undiluted system?). Overall, the elemental distribution in these 2 catalyst systems is homogeneous and the data obtained is comparable to EDX analysis.

Table 5.6: Molar ratio of elements normalized to Mo for undiluted system

Element	Atomic % for standard recipe A1	Atomic % for sample A2	Normalized to Mo		
			Theory	A1	A2
Mo	65.928	65.875	1.000	1.000	1.000
V	15.519	15.989	0.300	0.235	0.243
Te	11.750	10.198	0.230	0.155	0.155
Nb	6.803	7.938	0.125	0.103	0.121

Table 5.7: Molar ratio of elements normalized to Mo for diluted system

Element	Atomic % for standard recipe B1	Atomic % for sample B2	Normalized to Mo		
			Theory	B1	B2
Mo	58.705	56.920	1.000	1.000	1.000
V	7.933	7.692	0.300	0.255	0.255
Te	10.550	8.575	0.230	0.136	0.113
Nb	5.988	6.169	0.125	0.105	0.112
Si	16.650	20.570	-	0.969	1.234

5.2.4 FTIR

The chemical and structural changes taking place during the decomposition of the ligands under heat treatment can be observed from FT-IR spectroscopic analysis. This technique is useful to understand the changes of the ligands before and after calcination with respect tothe parameters being varied during preparation.. The FTIR measurement was carried out on all precursors and calcined samples

The IR spectra of the dried catalysts and catalysts after activation are given in Figure 5.22 Figure 5.23 respectively. According to the Botto and his group, these bands are related to the presence of $(NH_4)_6TeMo_6O_{24}.nH_2O$ which is an Anderson-type heteropolyanion (Botto, C.I. Cabello et al. 1997). The band at 3438 cm^{-1} is assigned to the asymmetric and symmetric O-H stretching modes of lattice water. Whereas, the bands at 3140 and 3014 cm^{-1} are due to symmetric and asymmetric stretching vibration of NH_4^+. Furthermore, the band at 1678 cm^{-1} which can be assigned to C=O stretching vibrations. Band around 1400 cm^{-1} can be ascribed to the asymmetric stretching vibrations of the tetrahedral ammonium ion (Botto, C.I. Cabello et al. 1997). Summary of the peaks observation for precursors and catalyst are tabulated in Tables 5.8 and 5.9.

Table 5.8: FTIR absorption band position and their assignments for sample prepared

Band position [cm^{-1}]	**Assignment**	
	Dried	**Calcined**
3138	(O-H) asy, sym stretching modes of lattice water	
3014,3140	Sym, asym stretching vibration of NH_4^+	
2802	C-H stretching vibration *(not from the sample but contaminate from the environment)*	
2914	-	-
1678	C=O stretching vibration	- decomposed
1639	H-O-H bending modes	
1400	NO_3^- bending vibration/ NH_4^+ bending vibration	- decomposed
1273	-	-
1116,1106, 460-472	Si-O stretching vibration	

Table 5.8: Band position for reference transition metal oxide

References		Observed	
Assignment	**Band position [cm^{-1}]**	**dried**	**calcined**
α-$TeMo_4O_{13}$	shoulder at 980	976	Disappear after calcinations
Mo-O vibrations	932, 545	932,545	558
Mo=O streching	920- 860 broad band	905	920,905
$TeMo_5O_{16}$	920	932	920
MoO_3	991,870	Not detected from the sample	Shoulder at 875
V=O V-O-Me (Me=Nb, Te)	915, 582, 454	558	457,575
Mo-O-Me (Me= Mo, Nb, Te) antisymmetric	751, 608	615	748
Mo-O-Me (Me=Nb, Te,V)	884, 792, 640	798, 685	748,794
H_2O librations	615	615	Disappear after calcinations
Vibrations of Mo-O, Te-O and/or Mo-O-Te	666,792	666,792	604

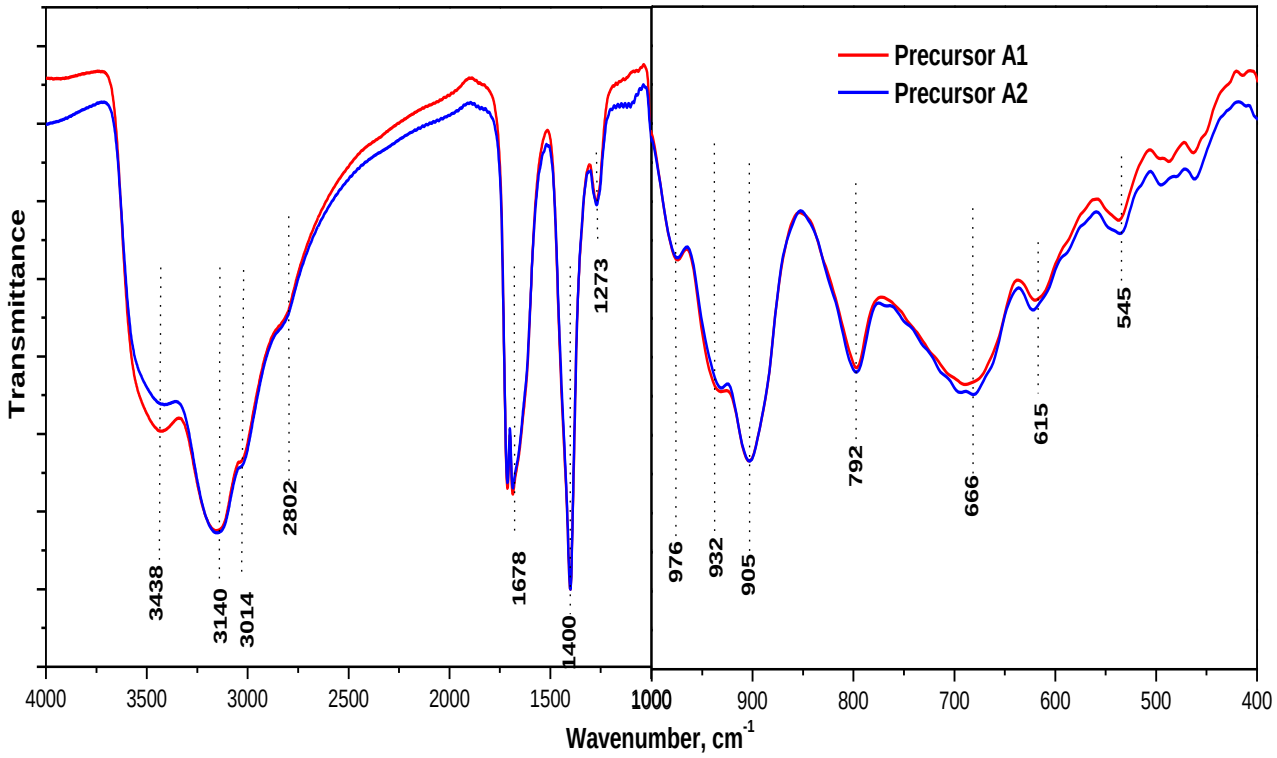

Figure 5.22: FTIR spectra precursor for undiluted system before calcined

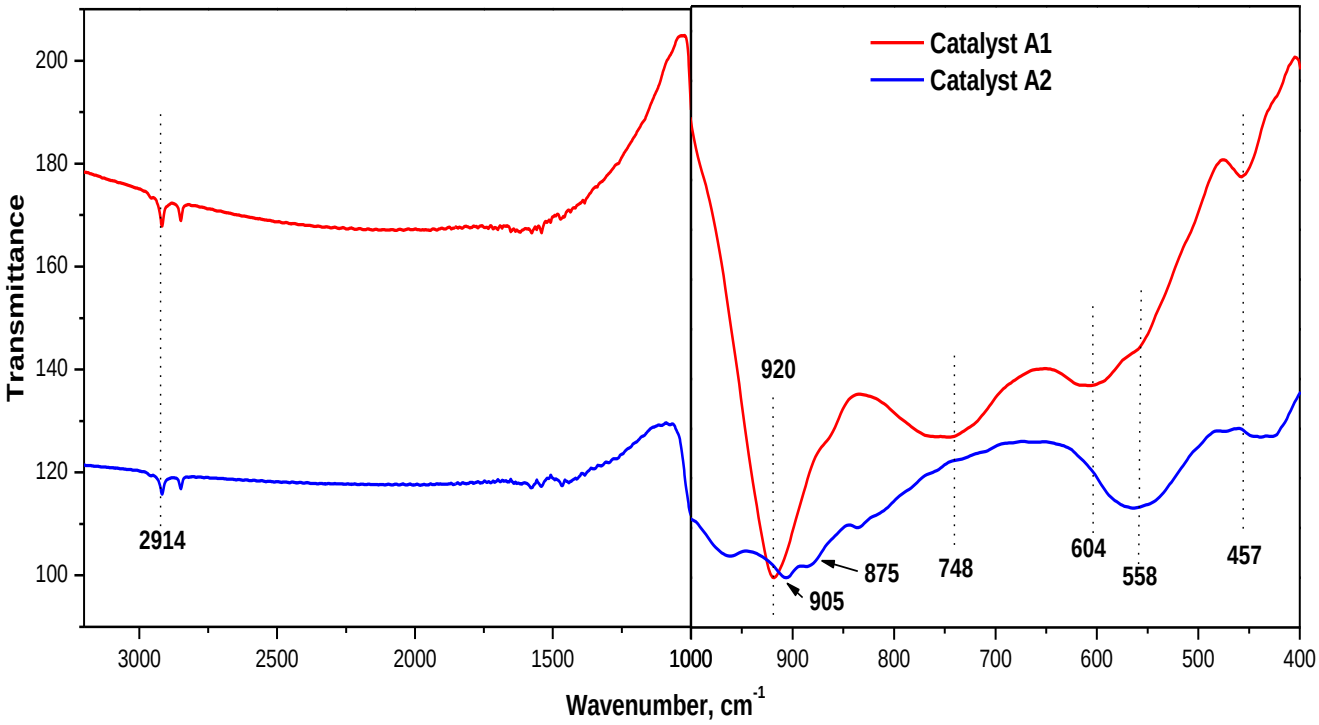

Figure 5.23: FTIR spectra catalyst for undiluted MoVTeNb oxide system after calcined

Figure 5.24 and 5.25 show the IR spectra for uncalcined and calcined samples**.** The diluted system shows obvious differences at low frequency region. The bands at 1095 and 1106 cm^{-1} are assigned to Si-O stretching and vibration of silica. On the other hand, the intense bands at 937, 920 and 545 cm^{-1} can be ascribed to Mo-O vibrations and the band at 920 cm^{-1} can be assigned to $TeMo_5O_{16}$. According to Botella and his co-worker, the bands at 792, 720 and 666 cm^{-1} can be assigned to Mo-O, Te-O and/or Mo-O-Te, while the band at 615 cm^{-1} represents H_2O liberations (Botella, Lopez Nieto et al. 2002). The summary of all bands appeared in the sample are tabulated in Tables 5.8.and 5.9

As a result, it can be summarized that the FT-IR analysis revealed that calcination procedure at 873 K for undiluted system and 923 K for diluted system are sufficient to remove all discernible traces of molecular inorganic/organic ligands with the disappearance of several bands contributed by the nitrate and water after calcinations.

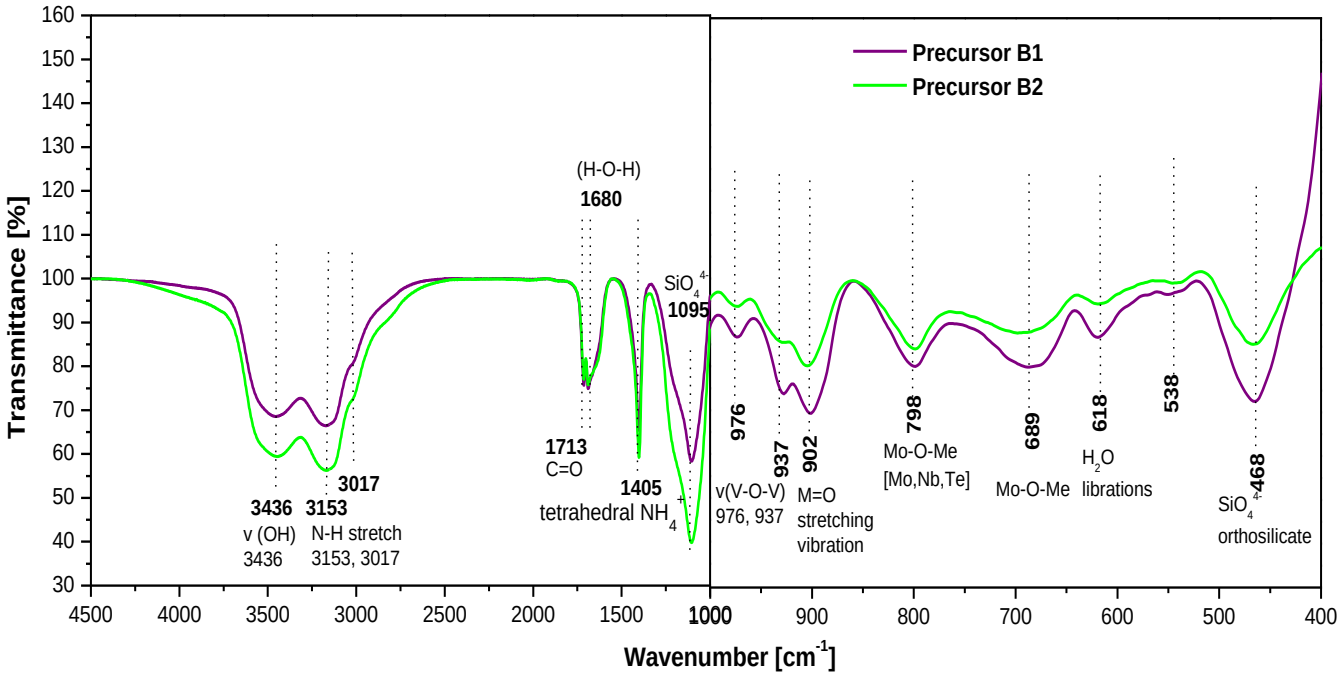

Figure 5.24: FTIR spectra precursor for undiluted MoVTeNb oxide system before calcined

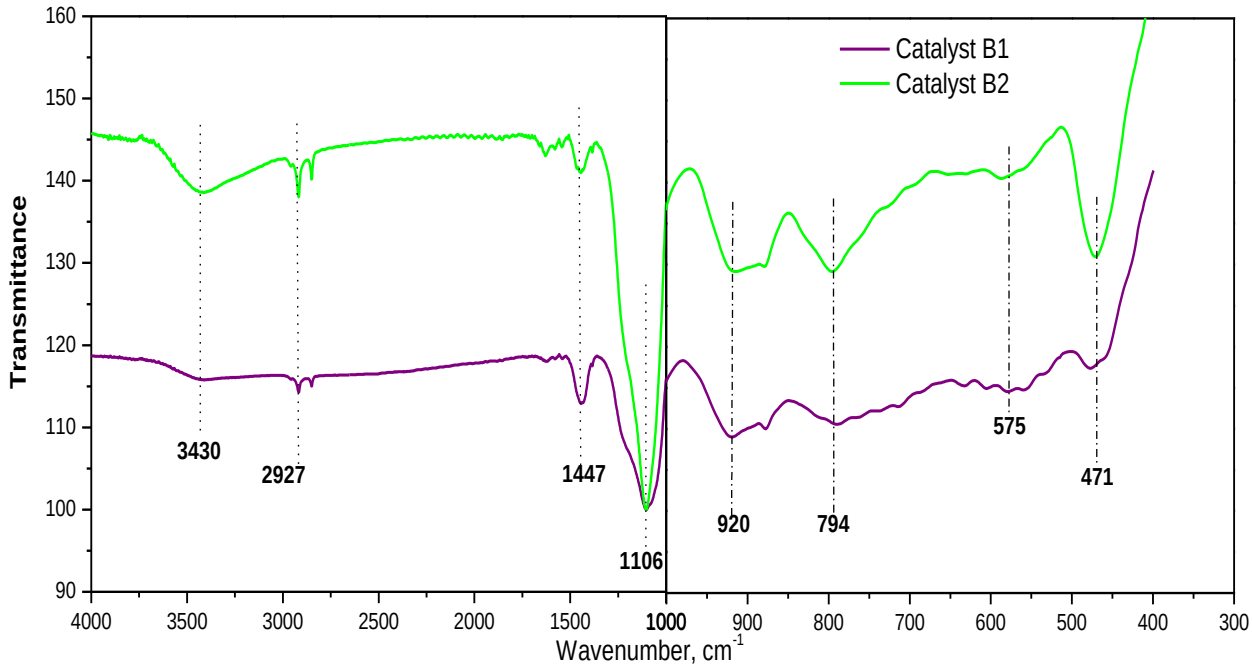

Figure 5.25: FTIR spectra precursor for diluted MoVTeNb oxide system after calcined.

5.2.5 BET

Nitrogen physisorption technique is used to define the textural properties of precursors and catalysts. The rate of the product formation is a function of the available surface area of the active phase and so it follows that the greater the amount of active surface area (ASA) accessible to the reactant, the higher is the reaction throughput. In supported systems, it is often customary to assume that a fixed relaxation exists between the total surface areas (TSA) and the ASA. It is of primary concerned to ensure that TSA is not lost during catalyst preparation. Thus, the mode of catalyst preparation and its subsequent activation greatly influences the resulted surface area on the catalyst system prepared. Therefore, it is useful to measure the surface area for each sample to evaluate and to develop the methodology used in the modification. The addition of reducing agent in the sample preparation is found to have little effect on surface area of the sample formed. Addition of

oxalic acid in undiluted MoVTeNb oxide has slightly increased the surface area from 3.3 to 5.9 $m^2 g^{-1}$; while the diluted system shows a more significant increment of surface area from 26.7 to 37 $m^2 g^{-1}$ after the addition of oxalic acid The BET results from the samples are summarized in Table 5.10 and the isotherms are depicted in Figures 5.26. The isotherms for all samples show similar hysteresis loop in region IV which is associated with capillary condensation taking place in mesopores, and the limiting uptake over a range of high P/P^o. The surface area increases for undiluted MoVTeNb oxide catalyst with addition of reductive oxalic acid. Addition of support (silica) has resulted in better distribution of the metal oxide on the surface of the silica particle that lead finally to an increase in the accessible metal oxide surface.

Table 5.10: Surface area for undiluted and diluted system

Sample	Type	Surface Area (m^2/g)
Catalyst A1	Undiluted	3.3
Catalyst A2		5.9
Catalyst B1	Diluted	26.7
Catalyst B2		37

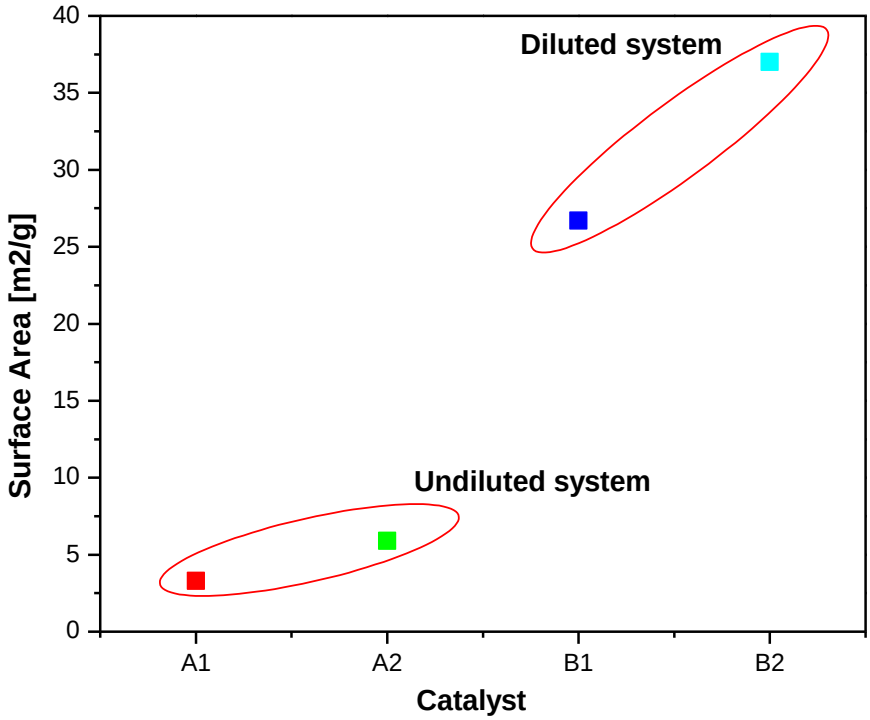

Figure 5.26: Distribution of surface area for undiluted and diluted MoVTeNbOx system

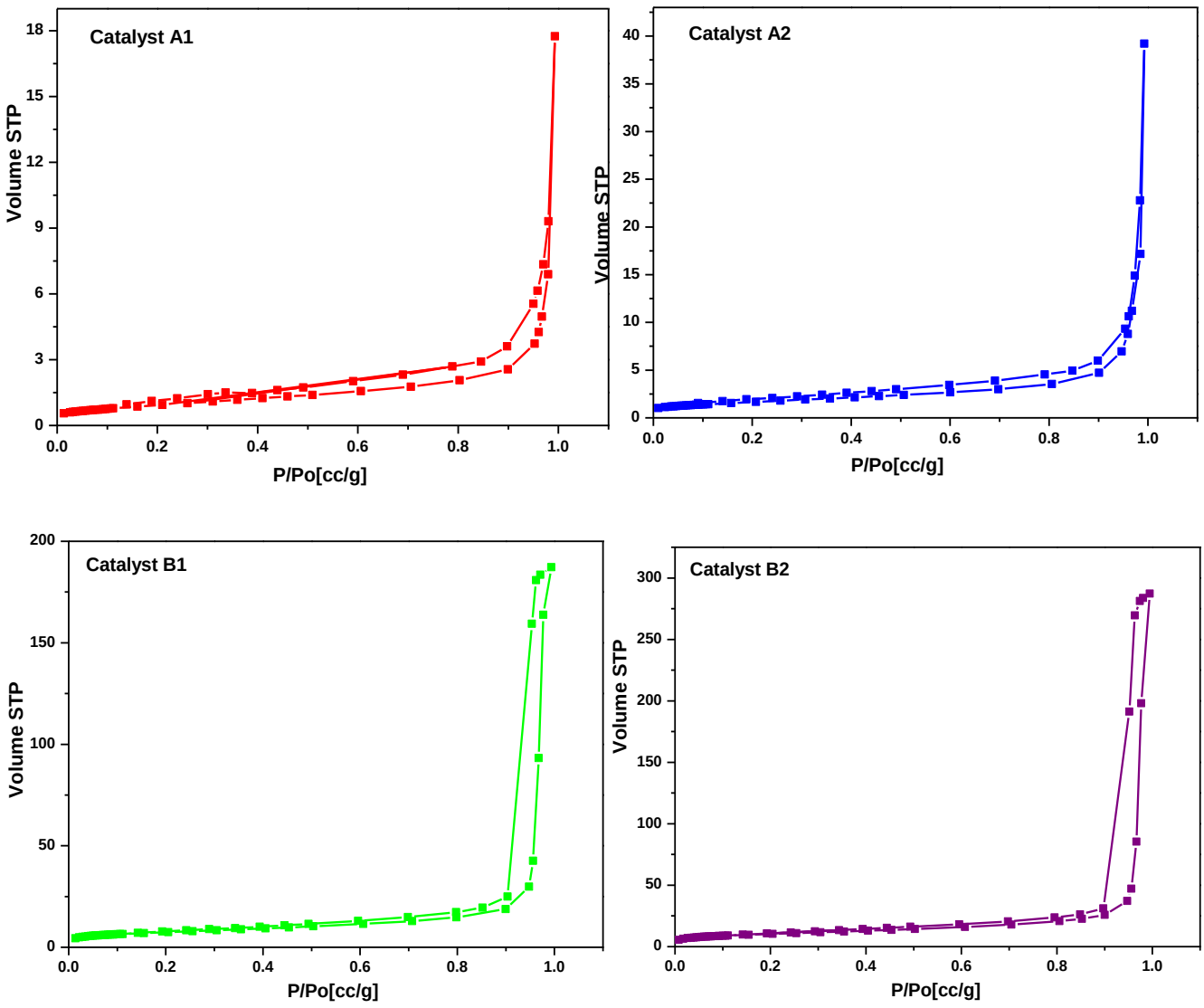

Figure 5.27: BET isotherm for undiluted (above) and diluted (below) system

5.3 Thermal Analysis

5.3.1 Thermogravimetric Analysis (TGA)

Thermal analysis is used to identify the sequence of events transforming the precipitate into active oxide. Thermal treatment in metal precursor is important to achieve a complete conversion of the precursor into a metal oxide in order to form an active catalyst for selective reaction to acrylic acid. One of the most critical preparation steps in this study is the calcination procedure. The lowest possible temperatures to achieve complete conversion of the precursors into oxides are required and a complete gasification of all volatile ligands is essential to form an active metals oxide.

The methodology of optimizing the calcination by thermal analysis would be greatly improved if a different atmosphere and inert could be applied to the system.Table 5.11 below shows the purpose of thermal analysis in this study.

Table 5.11: Purpose of DSC and TGA techniques

Thermal Analysis	Conditions	Purposes
DSC	Temp = 298 K to 873 K Rate = 5 K/min Gas = Compressed Air	To observe and confirm the temperature range of real activation tempoerature
TGA	1) Temp = 298 K to 548 K Rate = 10 K/min Gas = Compressed Air 2) Temp = 298 K to 873 K Rate = 2 K/min Gas = Argon	To observe the mass loss and gas evolve during real calcination

A series of sample and precursors of undiluted and diluted were measured using the TGA-MS and DSC method in order to obtain meaningful information on the nature of precursor presence and the decomposition processes via weight loss during heat treatment. The identification of gases evolved is important to postulate the reaction mechanism of the precursor during calcination. The first derivative of the TGA (DTG) was plotted to track changes in weight loss during analysis. Complementary with TGA techniques, DSC analysis was also performed with the same temperature programme.

There are two stages of TGA program involved in activation of sample. For undiluted system, the first temperature program was chosen at a linear ramp from 303 – 548 K with heating rate of 10 K/min and synthetic air flow rate of 100 ml/min. Secondly, temperature program was chosen with linear ramp from 373 up to 873 K at a heating rate of 2 K/min; argon flow rate of 100 ml/min coupled with powerful MS. For diluted sample, the temperature program was chosen at 303 -598 K with heating rate of 10 K/min and synthetic air flow rate of 100 ml/min and then changed to second temperature program at 373 – 923 K, flowing with 100 ml/min of Argon at heating rate 2K/min. This entire program was coupled with powerful MS detector to identify gases evolved from sample precursor during TGA analysis. The analysis data for TGA measurement is tabulated in Tables 5.12 and 5.13 whilst TGA curves are depicted in Figures 5.28 and 5.29.

Table 5.12: Weight loss at various steps and temperature under air flow as obtained from the thermal analysis data

Precursor	1st weight loss		2nd weight loss		3rd weight loss		Residue (%)
	T_R and T_{min} (K)	wt loss (%)	T_R and T_{max} (K)	wt loss (%)	T_R and T_{max} (K)	wt loss (%)	
Undiluted							
A1	T_R= 303- 423 T_{min}= 363	5.929	T_R= 423-603 T_{min}= 503	18.824	-	-	75.254
A2	T_R= 303-423 T_{min}= 358	6.108	T_R= 423- 573 T_{max}= 493	22.717	-	-	71.2481
Diluted							
B1	T_R= 303-423 T_{min}= 353	4.302	T_R= 423-503 T_{min}= 473	8.213	T_R= 503-623 T_{min}= 533	7.161	80.329
B2	T_R= 303-423 T_{min}= 353	4.123	T_R= 423-653 T_{min}= 473	11.892	-	-	83.985

Table 5.13: Weight loss at various steps and temperature under Argon flow as obtained from the thermal analysis data

Precursor	1st weight loss		2nd weight loss		3rd weight loss		Residue (%)
	T_R and T_{min} (K)	wt loss (%)	T_R and T_{max} (K)	wt loss (%)	T_R and T_{max} (K)	wt loss (%)	
Undiluted							
A1	T_R= 303- 773 T_{min}= 633	4.3557	-	-	-	-	97.4425
A2	T_R= 303- 643 T_{min}= 573	2.5958	T_R= 643-703 T_{min}= 673	0.8588	-	-	97.7906
Diluted							
B1	T_R= 303-443 T_{min}= 333	1.5083	T_R= 443-673 T_{min}= 623	0.3033	-	-	97.2095
B2	T_R= 303-473 T_{min}= 333	1.9100	T_R= 473-673 T_{min}= 633	0.3031	T_R= 473-900 T_{min}= 780	0.5284	97.3048

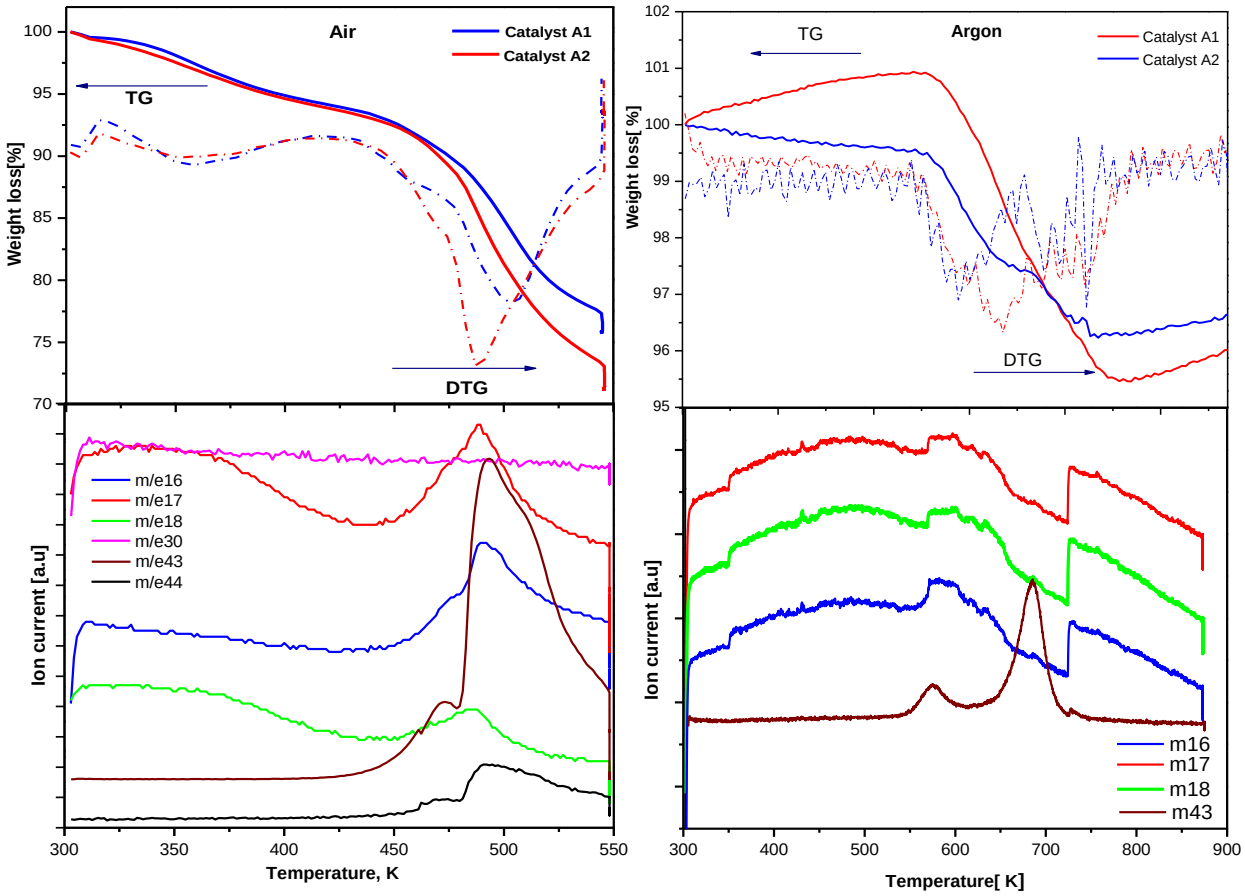

Figure 5.28: TG curve in air and argon flow of the undiluted MoVTeNb oxide system (top) TGA and DTG data; (bottom) MS traces of gas envolved

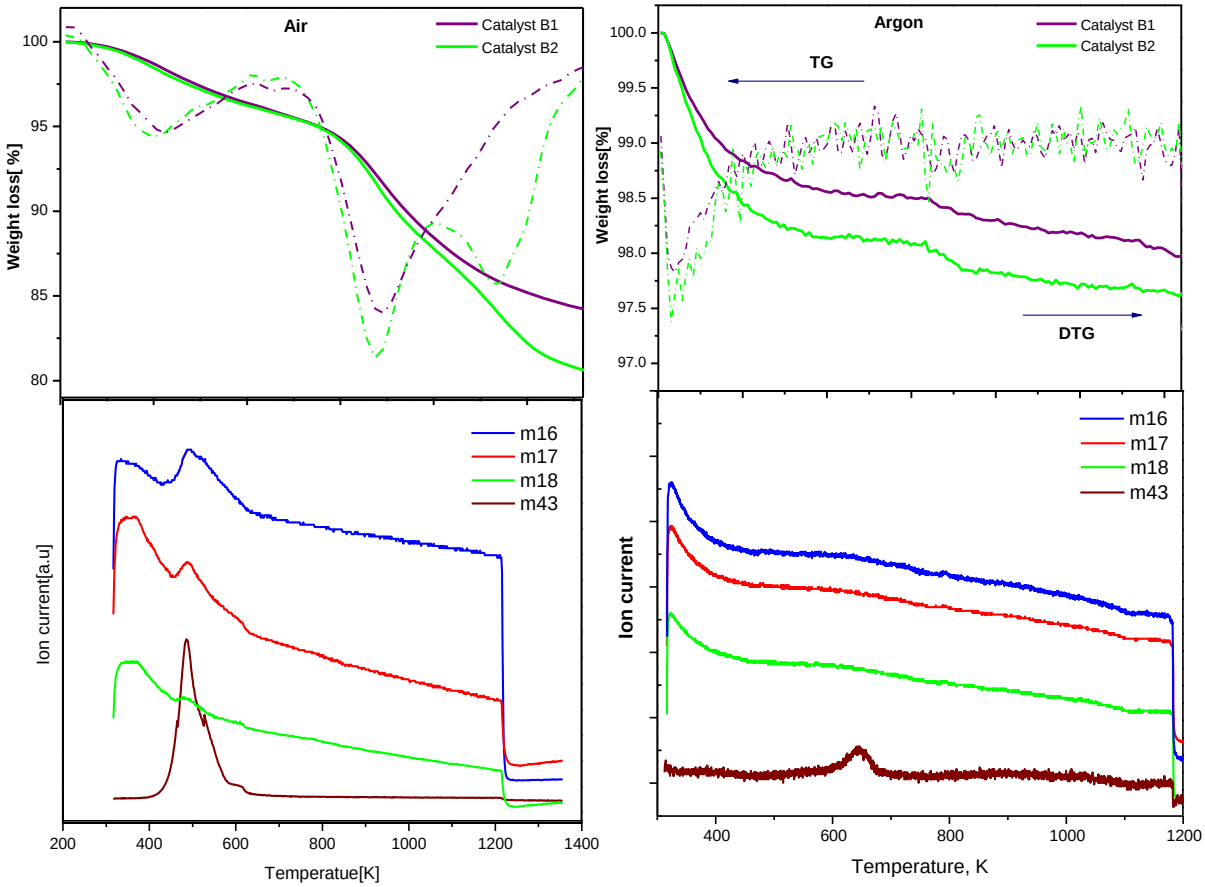

Figure 5.29: TG curve in air and argon flow of the diluted MoVTeNb oxide system (top) TGA and DTG data; (bottom) MS traces of gas envolved

The TGA data for undiluted and diluted $Mo_1V_{0.3}Te_{0.23}Nb_{0.125}Ox$ systems heating under air and argon is shown in Figure 5.27 and 5.28. From the result, an several trends were observed for all catalysts.Overall, similar trend could be observed for all the catalyst systems. Two endothermic signals with associated mass losses were observed when the catalysts were heated in air up to 548 K. The first endotherm occurrd at about 363 K is due to the desorption of water with a mass loss of about 6 %. From DSC, it is confirmed that water, carbon dioxide, ammonia and nitrate compound traces are decomposed at 503 K. The second endothermic signal has maxima 503 K with mass loss at about 19 %. This

weight lose can be attributed to the liberation of CO_2. -The mass scpectroscopy results indicate that the last endotherm shows mass/charge (*m/e*) signals for 16 and 18 (water), 17 (NH_3, when 17/16 signal ratio increases), (NOx) and 43 (CO_2 or perhaps N_2O) at 503 K. The NOx (*m/e* 30) signal was not detected from MS analysis. The signal for water has a maximum at 363 K, and the signal for NH_3 reaches a maximum at about 480 K. The signal for CO_2 (N_2O) shows a maximum at about 490 K. The two endotherms account for about 25 % mass loss and increased to 29% for sample with oxalic acid in the undiluted sample. However, the total mass losse for diluted sample is about 13 % and a slightly higher mass loss (16%) for sample with oxalic acid.

During the heat treatment in the inert gas (Argon) which is shown in Fig 5.28, there are 4 steps of weight loss. The 1st mass loss (4 %) happened at 550 K which is accompanied by an endothermic peak. Various peaks at m/e 16, 17 and 18 (consistent with water and perhaps some NH_3), and m/e 44 (N_2O or CO_2) could be observed from MS results at 550 K. The *m/*e 43 signals reach maxima at about 680 K, and *m/e* 16 & 17 and 18 signals reach maxima at about 600 K. For diluted sample, only m/e 43 signal reaches maxima at 680 K. The m/e 16,17 and 18 signals show no peak in MS analysis and it is believed that this sample has been dried completely and water was removed during pretreatment in air at 548 K or 598 K for diluted sample. The total weight loss for undiluted system is about 4.4 % and it is slightly lower (3.5 %) for catalyst A2. This mass loss occurs at temperature in the range of 550 to 700 K. However, only 1.5 % weight loss for catalyst B1 and 1.9 % for catalyst B2 for the first step in mass loss at temperature range 303-473 K. The next step for mass losses of catalyst A2 is 0.86 % centered at 603 K indicates *m/e* signals 43 (N_2O). While only 0.3 % mass loss for catalyst B1 at temperature 443-673 K and 0.83 % for

catalyst B2 at temperature range 473 – 673 K. The final mass loss centered at about 780 K constitutes 0.52 % shows no gas products. The lack of a signal in MS indicates that the gas phase products, most likely sub-oxides, condensed before MS inlet.

5.3.2 Differential Scanning Calorimetry (DSC)

The TGA-MS analysis is supported by the DSC analysis that gives the enthalpy value of endothermic and exothermic reaction happened during the temperature programmed analysis. As described in the methodology section, the activation procedure of the $Mo_1V_{0.30}Te_{0.23}Nb_{0.125}O_x$ precursor was carried out in two-steps calcinations. The same temperature programmed was applied in samples calcination and DSC analysis. Based on the DSC measurement data, both the enthalpy of dehydration and ligand decomposition of all precursors (A1, A2, B1 and B2) were calculated and the data is tabulated in Table 5.14. The patterns in Figure 5.29 describe the thermal events of different preparation methods. Overall, The entire figure shows 4 typical transitions The DSC patterns in Figures 5.30 and 5.31 performed and endothermic net energy change to the undiluted & diluted spray dried precursor (catalyst A1, A2, B1 & B2) at low temperature range from 330 – 450 K in the first transition. This is associated with the total amount of water released from the sample with an endothermic entalphy 81.57 Jg^{-1}. These effects are also relevant to catalyst A2 (149.08 Jg^{-1}), B1 (145.78 Jg^{-1} and B2 (182.54 Jg^{-1}) at first endothermic around 450 K. At the second transition for all dried precursor, the main change occurs at 450 – 530 K can be associated with several processes with an endothermic energy balance due to the evaporated and decomposed of ligands such as water and ammonia. This is because the sample itself contains structural water from the metal salt and removable ligands. In this

temperature region, two endothermic events occurred for catalyst A1 and B1 An endothermic event can be seen in DSC signals for sample A2 and B2 which were added with reducing agent i.e. oxalic acid. In the presence of oxalic acid, the sample shows a pronounced change on the chemical and phase transformations of the sample.

Water, carbon dioxide, ammonia and nitrogen oxides are the ligands released by oxidation of redox-active ligands at the endothermic and exothermic effect at temperature range around 530 – 650 K respectively and it can be clearly seen in DSC signals as third transition phase. When thermal decomposition happened, this phase is being coupled with the deammoniation. There are two types of deammoniation ie. the oxidation and decomposition of ammonia. The transformation is always accompanied by the decomposition of a small amount of ammonium ions. During exothermal changes, the endothermal deammoniation can be overlapped on the same time. Nevertheless, deammoniation must be endothermic and the transformation is essential in solid phase. The small deammoniation can be considered as an evolution of ammonia impurities induced by the crystal rearrangement. The detection of carbon dioxide in MS and DSC signal is detected for decomposition of oxalate and nitrogen oxides are formed from the oxidation of ammonia and the reduction of molybdenum and vanadium precursors. The water observed at higher temperatures may be formed upon condensation processes and therefore is classified as structural water. This exothermic effect is associated with a crystallization process as revealed by SEM and XRD.

The final transition of thermal analysis can be considered as a solid state transformation producing endothermic and exothermic signals in DSC curves. The heat capacity of the

system changes significantly as seen in the baseline of the DSC. It is happened at above 600 K which leads to the formation of an extended solid with proper crystal structures whereas at low temperature the structures are still in supramolecular phase with a poly-ionic molecular structure and small volatile species as counter ions(Qureishah 2004). In this stage, there was no weight loss occurred from TGA analysis and can be concluded as onset temperature for crystallization. This can be referred as the active phase which is also known as M1 phase where phase transformation occurred during activation process.It indicates that the structure of whole metal-ligand system was strongly bounded and well restructured during calcination process. These observations can be confirmed by XRD analysis where the active M1 phase exhibits the crystal structure after calcination.

In summary, the DSC results clearly revealed that the sequence of events occurred during thermal evolution. Thus, DSC technique can be considered the best tool to confirm the 'real' calcination temperature instead of complex interplay of ligands removal, polycondensation and phase transformation become stable phase occurred in several temperature.

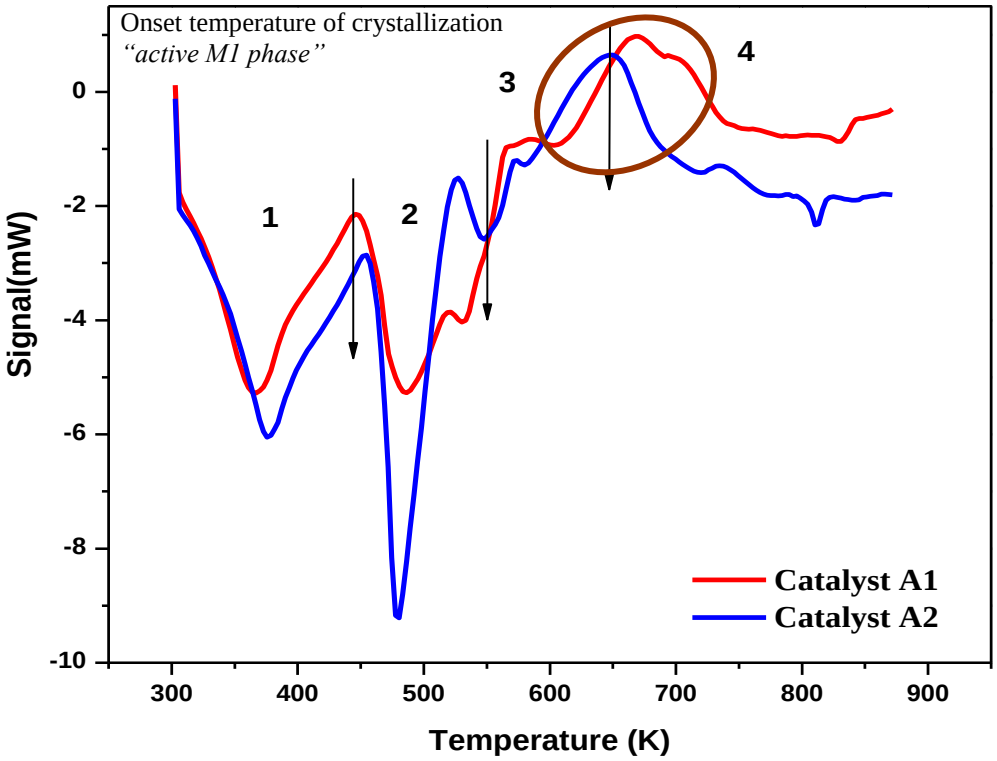

Figure 5.30: DSC signal of catalyst A1 and catalyst A2 (with oxalic acid) in undiluted system

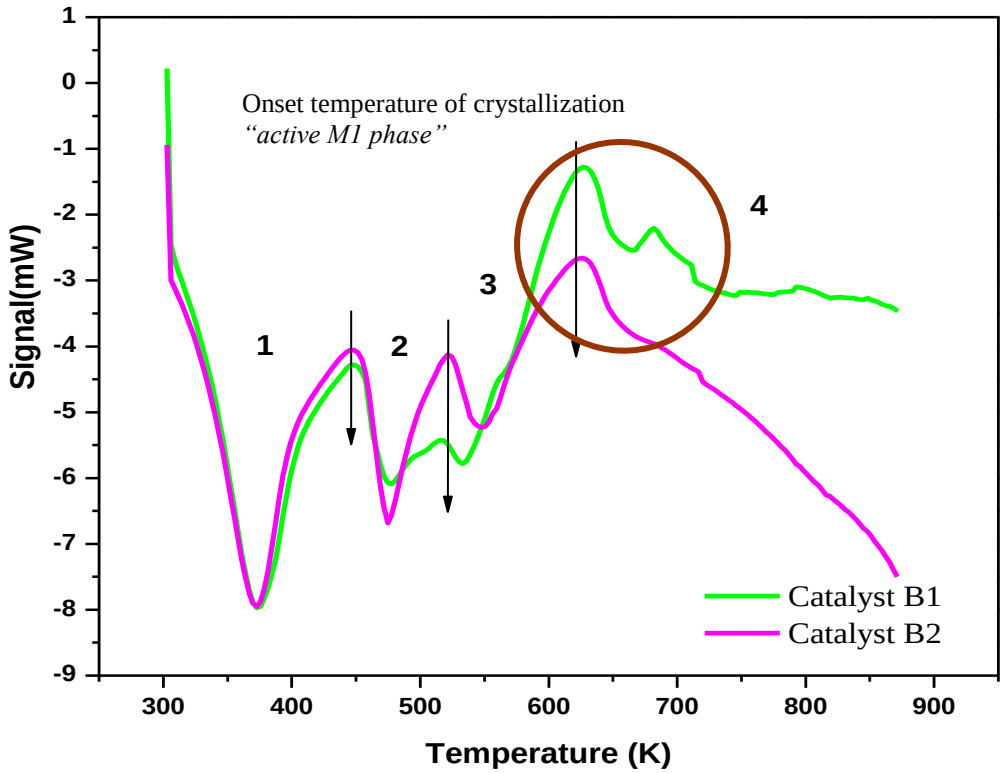

Figure 5.31: DSC signal of catalyst B1 and catalyst B2 (with oxalic acid) in diluted system

Table 5.14: DSC temperature profiles for all undiluted and diluted MoVTeNb oxide catalyst

Dried samples	DSC							
	1st Transition		**2nd Transition**		**3rd Transition**		**4th Transition**	
	T_R and T_{endo} (K)	ΔH / Jg^{-1}	T_R and T_{endo} (K)	ΔH / Jg^{-1}	T_R and $T_{endo/exo}$ (K)	ΔH / Jg^{-1}	T_R and $T_{endo/exo}$ (K)	ΔH / Jg^{-1}
Undiluted System								
Catalyst A1	T_R = 330.20- 435.97 T_{endo} = 365.68	-81.57	T_R = 469.07 – 511.69 T_{endo} = 484.47	-89.93	T_R = 526.38 – 563.68 T_{endo} = 605.44	-16.89	Phase transformation Exothermic	
Catalyst A2	T_R = 330.53- 426.61 T_{endo} = 374.57	-149.08	T_R = 465.50- 516.86 T_{endo} = 480.02	-133.82	T_R = 530.19- 568.93 T_{endo} = 546.87	-17.55	Phase transformation Exothermic	
Diluted System								
Catalyst B1	T_R = 305.7 – 435.97 T_{endo} = 371.59	-145.78	T_R = 458.86 – 496.35 T_{endo} = 474.52	-21.54	T_R = 521.89- 558.43 T_{endo} = 531.12	-9.28	Phase transformation Exothermic	
Catalyst B2	T_R = 323.61- 409.32 T_{endo} = 370.35	-182.54	T_R = 459.86- 506.04 T_{endo} = 474.52	- 52.86	T_R = 532.13- 560.9 T_{endo} = 546.67	- 41.01	Phase transformation Exothermic	

5.3.3 Temperature Programmed Reduction (TPR)

Investigation of reduction behaviour through temperature programmed reduction (TPR) experiments is very useful to predict the catalytic potential of the catalyst (Repeated statement!) The narrow and symmetrical TPR profile and the low onset reduction temperature are characteristics of the good catalyst.

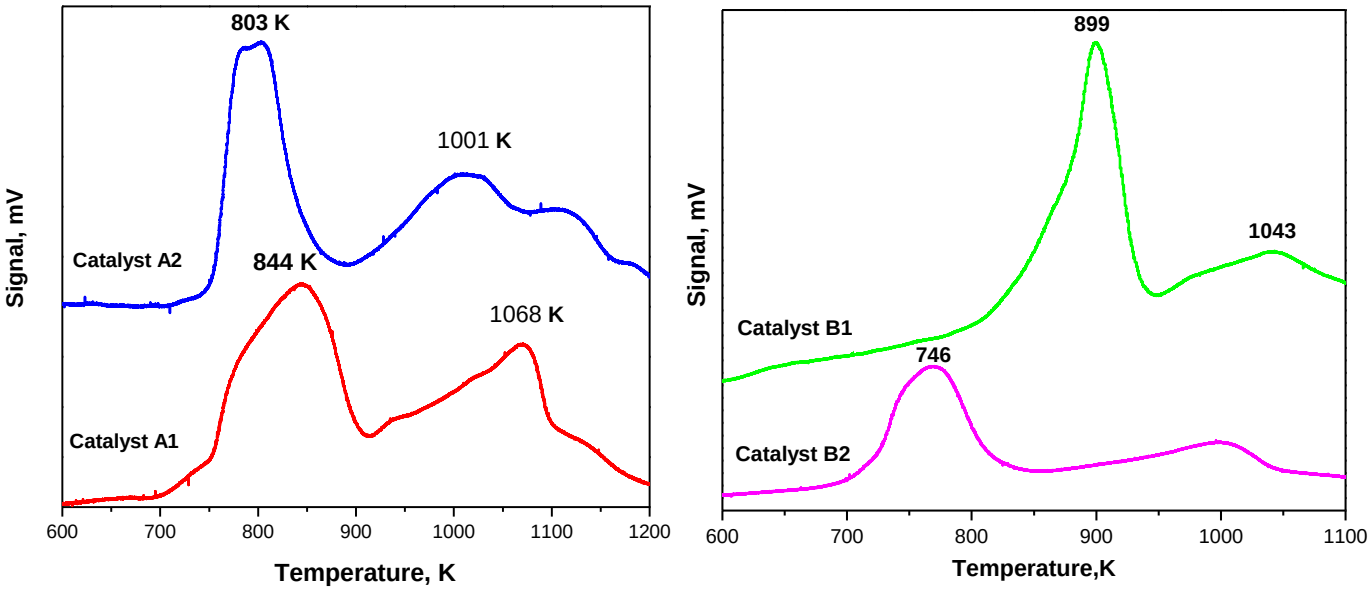

Figure 5.32: Temperature-programmed reduction profile for undiluted catalyst A1 and A2 (left) and diluted catalyst B1 and B2 (right) MoVTeNb oxide catalyst.

Figure 5.32 reports the TPR profile of samples for undiluted and diluted MoVTeNb oxide catalyst. H_2-TPR profiles and amount of H_2 consumption of undiluted and diluted MoVTeNb oxide samples were shown in Figure 5.30. This TPR profile can give some information in order to quantify the amount of labile oxygen. As Figure 5.30 (top) showed two peaks in the H_2-TPR pattern of standard recipe (Catalyst A1) and modified catalyst (Catalyst A2). The first temperature was reduced for standard recipe (A1) at maximum

temperature 803 K about 38 % and slightly increased to 63 % for A2 at 844 K. The sample A2 exhibited the greatest reducibility of lattice oxygen, whereas A1 was less and mostly difficult to reduce. It might because the presence of oxalic acid as reducing agent in sample A2. Furthermore, one sharp peak in the range 790 – 900 K for diluted samples can be observed in the H_2-TPR profiles. For B1 sample, the sharp peak at 899 K showed the oxygen was removed about 58 % while 100 % of oxygen removed for B2 and shifted to higher temperature at 793 K. The effect of oxalic acid as reducing agent can be clearly seen in sample B2 whereby most of the oxygen was being removed from the sample. This first peak (at what temperature?) is assigned to surface terminal oxygen atoms of an oxide but some oxygen may also be available from sub-surface layers by diffusion. It is known that the Mo^{6+} and V^{5+} are reduced more easily in multi metal oxide (MMO) solid solution than in pure MoO_3 and V_2O_5 (Baiker and D.Monti 1985).

The next temperature of removable oxygen can be seen at temperature range 1000-1070 K for both systems. The H_2-TPR profiles of A1 shows increment of removable oxygen about 62 % compared to A2 which is only 37%. The broad peak at temperature 1043 K is observed with 42 % of oxygen removed from B1 sample. Nevertheless, no removable oxygen detected in sample B2. At this temperature region, the peaks could be mainly ascribed to the reduction of V and Mo species (Jiang, W.Lu et al. 2004). The total amount of removed oxygen atom and labile oxygen are tabulated in Table 5.15. The amount of labile oxygen removed is 2.1×10^{20} (**A1**), 2.4×10^{20} (**A2**), 1.5×10^{20} (**B1**) and 1.8×10^{19} (**B2**). The reducibility of labile oxygen was removed from undiluted sample are increased after addition of oxalic acid during preparation methods. Nevertheless, it was slightly decreased for diluted sample. The presence of silica decreased the reductive stability. From

the TPR result, in both undiluted and diluted system it was observed that the addition of reducing agent influenced the redox properties of the system.

Table 5.15: Total number of oxygen atoms removed from the catalysts by H_2 and the labile oxygen.

Catalysts System	T_m (K)	Oxygen atoms removed (%)	Oxygen atoms removed (mol g^{-1})	Oxygen atoms removed (atoms g^{-1})	Labile Oxygen (atoms m^{-2})
Undiluted					
A1	803	38.2	2.9×10^{-3}	4.6×10^{20}	7.91×10^{19}
	1001	61.8	4.7×10^{-3}	7.5×10^{20}	1.3×10^{20}
Total oxygen atoms removed			7.6×10^{-3}	1.2×10^{21}	**2.1×10^{20}**
A2	844	62.9	3.1×10^{-3}	4.9×10^{20}	1.5×10^{20}
	1068	37.1	1.8×10^{-3}	2.9×10^{20}	8.8×10^{19}
Total oxygen atoms removed			4.9×10^{-3}	7.9×10^{20}	**2.4×10^{20}**
Diluted					
B1	899	58.4	1.4×10^{-2}	2.3×10^{21}	8.7×10^{19}
	1043	41.16	1.0×10^{-2}	1.6×10^{21}	6.1×10^{19}
Total oxygen atoms removed			2.5×10^{-2}	4.0×10^{21}	**1.5×10^{20}**
B2	746	100	4.2×10^{-3}	6.8×10^{20}	1.8×10^{19}
Total oxygen atoms removed			4.2×10^{-3}	6.8×10^{20}	**1.8×10^{19}**

[a] Surface areas: A1 = 3.3 $m^2 g^{-1}$, A2 = 5.9 $m^2 g^{-1}$,B1 = 26.7 $m^2 g^{-1}$, and B2= 37.0 $m^2 g^{-1}$.